TIC

NUREG/CR-0907
TREE-1374
for U.S. Nuclear Regulatory Commission



# POWER-COOLING-MISMATCH TEST SERIES
# TEST PCM-1
# FUEL ROD BEHAVIOR REPORT

DANIEL T. SPARKS CLIFFORD J. STANLEY



August 1979

EG&G Idaho, Inc.

IDAHO NATIONAL ENGINEERING LABORATORY

DEPARTMENT OF ENERGY

IDAHO OPERATIONS OFFICE UNDER CONTRACT DE-AC07-76IDO1570

Available from
National Technical Information Service
Springfield, Virginia 22161
Price: Printed Copy A03; Microfiche $3.00

The price of this document for requesters outside the North American continent can be obtained from the National Technical Information Service.

NUREG/CR-0907
TREE-1374
R3

# POWER-COOLING-MISMATCH TEST SERIES
# TEST PCM-1
# FUEL ROD BEHAVIOR REPORT

Daniel T. Sparks
Clifford J. Stanley

**EG&G Idaho, Inc.**
**Idaho Falls, Idaho 83401**

Published August 1979

PREPARED FOR THE
U.S. NUCLEAR REGULATORY COMMISSION
AND THE U.S. DEPARTMENT OF ENERGY
IDAHO OPERATIONS OFFICE
UNDER CONTRACT NO. DE-AC07-76IDO1570
NRC FIN NO. A6041

# ABSTRACT

The fuel rod behavior results of the Power-Cooling-Mismatch (PCM) Test Series, Test PCM-1 are presented. The objectives of the test were to evaluate the behavior of a pressurized water reactor (PWR) type fuel rod operated at high temperatures in film boiling for a time beyond rod failure with large local regions of molten fuel, and to evaluate the consequences of the continued operation.

Test PCM-1, conducted in the Power Burst Facility, employed one 0.914-m-long PWR-design fuel rod, fabricated from unirradiated zircaloy-4 and pressurized to 2.58 MPa with a fill gas of 77.7% helium and 22.3% argon. The rod was subjected to a preconditioning period and a power ramp to 69 kW/m rod peak power at a constant mass flux of 1110 kg/s·m$^2$. The power was subsequently adjusted to 78 kW/m. The rod underwent film boiling during the power ramp to 69 kW/m and failed about 500 seconds later (about 470 seconds of film boiling operation at the peak temperature location). The test rod was in film boiling for 900 seconds with up to 85% of the local fuel pellet radius molten. The test information extends the existing PCM data base to include film boiling operation of a single fuel rod for a significant time beyond failure.

This report contains a description of the experiment, the test conduct, and the fuel rod behavior results. Measurement information, posttest examination results, and calculations from a transient fuel rod behavior code are used to interpret the test.

# SUMMARY

The Power-Cooling-Mismatch Test Series is being conducted by the Thermal Fuels Behavior Program of EG&G Idaho, Inc. This test series is part of the United States Nuclear Regulatory Commission's Fuel Behavior Program and is directed toward providing a base of experimental data for the development and assessment of analytical models on fuel rod behavior during normal and off-normal operating conditions. The objectives of Test PCM-1, the subject of this report, were to evaluate the behavior of a PWR-type fuel rod subjected to high temperature film boiling operation for a time beyond failure, with large local regions of molten fuel providing the potential for energetic molten fuel-coolant interaction upon failure. Specific areas of investigation were (a) the time to rod failure, (b) the mechanism of failure, (c) the potential for molten fuel related failure and energetic molten fuel-coolant interaction, and (d) the consequences of continued film boiling operation beyond rod failure.

Test PCM-1 was conducted in the Power Burst Facility at the Idaho National Engineering Laboratory. The single fuel rod used in this experiment was fabricated from unirradiated zircaloy-4 cladding and $UO_2$ fuel. The fuel rod had an active fuel stack length of 0.914 m and was pressurized to 2.58 MPa with a mixture of helium and argon gas (77.7% He and 22.3% Ar), the purpose of which was to simulate an end-of-life gas conductivity typical of a commercial PWR fuel rod.

The film boiling test phase was preceded by 16 hours of nuclear operation, which included power calibration and preconditioning periods at test rod peak powers up to 57 kW/m. Film boiling was induced by rapidly increasing the test rod peak power from 39 to 69 kW/m at constant coolant conditions (1110 $kg/s \cdot m^2$ mass flux, 605 K inlet temperature). The test rod power was subsequently adjusted to 77.8 kW/m for the duration of the film boiling test phase. The rod was operated in film boiling for a total time of 900 s with nominal coolant conditions of 15.2 MPa system pressure, 605 K inlet temperature, and 1050 $kg/s \cdot m^2$ shroud coolant mass flux. Rod failure occurred 520 s after the start of the power ramp to 69 kW/m (500 s after the first indication of film boiling) due to cladding embrittlement and, as a result, the bottom rod segment dropped 2.7 mm in the shroud. Molten fuel extending to 50% of the pellet radius and cladding temperatures of 1850 K at the time of failure were predicted; however, posttest evidence of molten fuel extending to 85% of the local pellet radius was observed. No energetic reactions as a result of the failure or subsequent rod breakup were observed. Cladding collapse onto the fuel stack resulted in greatly restricted fill gas communication between the failure location and other parts of the fuel rod. The fuel rod failure did not significantly degrade the coolability of the rod during film boiling operation, even though some disintegration of the cladding occurred. Shutdown of the reactor and ensuing rewet of the rod resulted in additional rod breakup and an 80% reduction in the shroud coolant flow. Twenty-four percent of the original fuel stack fragmented or powdered into pieces smaller than 76 μm and was washed out of the flow shroud by the coolant. However, cladding segments that had been completely oxidized, and cladding sections that had been previously molten (inside a shell of oxide) remained intact following rewet and posttest handling.

The overall behavior of the Test PCM-1 fuel rod prior to failure was not significantly different from that observed in previous PCM single-rod tests. The duration that the rod was subjected to high temperatures resulted in extensive damage to the fuel rod, but did not result in any discernible energetic molten fuel-coolant interaction or degradation of coolability during operation.

# CONTENTS

## FIGURES

## TABLES

# POWER-COOLING-MISMATCH TEST SERIES
# TEST PCM-1
# FUEL ROD BEHAVIOR REPORT

## I. INTRODUCTION

Projected growth of the nuclear power industry in the United States requires continuing investigations of the likelihood and consequences of potential reactor accidents in order to better quantify their potential effects on public health and safety. Essentially all such hypothesized accidents involving the cores of light water reactors (LWRs) are due to an imbalance between the heat generation rate in the fuel and the heat removal capacity of the coolant. The extreme cases have traditionally been designated the loss-of-coolant accident in which part or all of the core coolant would be lost, and the reactivity initiated accident in which a sudden, severe increase in power occurs due to the ejection of a control rod. Between these two extremes, LWR accidents which would result in off-normal power-cooling conditions are generally termed power-cooling-mismatch (PCM) accidents. Numerous credible single and coincident initiating events that may lead to PCM accidents can be postulated. For example, overpower events could result from malpositioned or unplanned withdrawal of control rods, xenon instability, loading and operation of a fuel assembly in an improper location (enrichment error), decreases in the reactor coolant soluble poison concentration, increased reactor coolant flow rate, or low temperature of the inflowing coolant caused by startup of an inactive loop at an incorrect temperature. Undercooling can be caused by a spectrum of coolant flow reduction incidents resulting from various primary pump malfunctions or electrical power losses, localized flow blockages, or secondary system malfunctions that result in increased or decreased heat removal from the primary coolant system. If departure from nucleate boiling (DNB) occurs during a PCM event, fuel rod damage and subsequent release of radioactivity into the primary system may occur.

The Power-Cooling-Mismatch Test Series is being conducted by the Thermal Fuels Behavior Program of EG&G Idaho, Inc., as part of the U.S. Nuclear Regulatory Commission's Fuel Behavior Program[1]. These tests are being performed to characterize the behavior of unirradiated pressurized water reactor (PWR) type fuel rods at power densities and flow conditions ranging from normal operating conditions to beyond the occurrence of DNB. The test series is directed toward providing an experimental data base to satisfy one of the major objectives of the Fuel Behavior Program - the development of analytical models of fuel rod behavior during normal and off-normal operating conditions.

Four categories of possible post-DNB fuel rod behavior during a PCM event have been identified, as shown in Table I. The physical processes that determine the particular category of expected post-DNB fuel rod behavior during a PCM event are zirconium phase change; the degree of zirconium-water and zirconium-fuel reaction, both of which influence cladding ductility; and fuel melting. The principal variables that control these processes are cladding temperature, the time at temperature, and rod power. The test series was designed as a parametric evaluation of fuel rod behavior response during film boiling, with cladding temperature, time in stable film boiling, and rod power as the primary variables, as outlined in Table II. Reference 2 provides a summary of results from previous PCM experiments.

The purpose of this report is to present the fuel rod behavior results of Test PCM-1. The objective of this test was to evaluate the behavior of a single PWR-type fuel rod subjected to high power operation in film boiling beyond the time of rod failure. Specific areas of investigation were: (a) the time to rod failure, (b) the mechanism of rod failure, (c) the potential for molten fuel related rod failure and energetic molten fuel-coolant interaction, and (d) the consequences of operating a rod in film boiling for a significant time following failure. The test information obtained extends the present single-rod PCM data base to include fuel rod behavior following failure at power. The data used as a basis for this analysis of the test results are reported in the experiment data report for Test PCM-1[3]. The results of the posttest metallurgical examination are presented in detail in the fuel rod material behavior report for Test PCM-1[4].

TABLE I

CATEGORIES OF POST-DNB FUEL BEHAVIOR DURING A PCM EVENT

| Category | Cladding Temperature Range (K) | Stabilized Zircaloy Cladding Phase | Zircaloy-Water Reaction | Cladding Ductility | Potential Fuel Rod Failure Modes |
|---|---|---|---|---|---|
| 1 | < 810 | Low $\alpha$ | None | Normal | None for unirradiated fuel rods. |
| 2 | 810 to 1105 | High $\alpha$ | None | High | Large deformations to rupture[a]; fuel melting. |
| 3 | 1105 to 1245[b] | Alpha plus beta transition | Minimal | Low | Small deformations to rupture[a]; fuel melting. |
| 4 | > 1245 | $\beta$ | Severe | High to low[c] | Cladding oxidation and embrittlement; fuel melting if powers are relatively high. |

a. Cladding ballooning is unlikely and is possible only after the rod internal pressure exceeds the system pressure.

b. This temperature range is intended to bound the cladding ductility minimum that occurs during the $\alpha + \beta$ phase transition.

c. The cladding ductility is initially high in $\alpha$-zircaloy, but will decrease rapidly as the zircaloy is embrittled by oxidation and oxygen absorption.

In Test PCM-1, a single, unirradiated fuel rod was contained in a circular flow shroud and positioned within the PBF in-pile tube. Nominal PWR coolant conditions (pressure and inlet temperature) were maintained in the in-pile tube throughout the nuclear testing. The test was conducted in three phases: power calibration, test rod preconditioning, and film boiling operation. Film boiling operation was initiated by rapidly increasing the test rod peak power from a steady state value of 39 kW/m to 69 kW/m at constant coolant conditions of 15.2 MPa pressure, 605 K inlet temperature, and 1110 kg/s·m$^2$ mass flux. After about 240 s, the test rod power was increased to 77.8 kW/m for the duration of the experiment. A description of the experiment configuration, test conduct, and test thermal-hydraulic conditions is presented in Section II.

The fuel rod response during film boiling operation is presented in Section III. In-pile measurements and postirradiation examination results are used as a basis for determining the fuel rod behavior during

TABLE II

PCM TEST PROGRAM DESCRIPTION

| | Test | | | | | | |
|---|---|---|---|---|---|---|---|
| | PCM-1 | PCM 2-A | PCM-2 | PCM-3 | PCM-4 | PCM-5 | PCM-7 |
| Number of test rods | 1 | 1 | 4[a] | 4[a] | 4[a] | 9 | 9 |
| Temperature stabilization category[b] | 4 | 2 | 2 | 3 | 4 | 4 | 4 |
| Maximum time of stable film boiling (s) | 900 | 210 | 117 | 45 | 160 | 660 | 660 |
| Maximum linear peak power (kW/m) | 78 | 58 | 51 | 54 | 68 | 58 | 58 |
| Number of DNB cycles | 1 | 9 | 8 | 5 | 4 | 1 | 3 |

a. Four test rods situated in a square array with individual flow shrouds.

b. Categories are from Table I and are original target values. The actual temperatures attained are listed in the individual test results reports.

film boiling operation. State-of-the-art fuel rod response code calculations (FRAP-T4)[a,5] are compared with measurement information to arrive at cladding surface temperature estimates for the Test PCM-1 film boiling operation. The temperature estimates were then used to evaluate the Test PCM-1 data relative to a cladding oxidation embrittlement criterion.

The Test PCM-1 results are discussed in Section IV. The fuel rod response measurements and posttest examination results are interpreted to determine the fuel rod behavior during Test PCM-1. New information obtained from the experiment is specifically detailed.

Conclusions regarding the test rod response and consequences of operation beyond failure during a PCM event are presented in Section V.

Detailed support information for this report is contained in the appendices, which are provided on microfiche attached to the inside of the back cover. Appendix A contains a detailed experiment description, including test assembly and instrument descriptions. The methods of determining test rod powers (and uncertainties) are contained in Appendix B. A description of the FRAP-T model and test data comparisons with the fuel rod response computer code are presented in Appendix C. Pretest fuel rod characterization information is contained in Appendix D.

a. FRAP-T4 MOD004, Version 09/14, MATPRO MOD010, Idaho National Engineering Laboratory Configuration Control Number H00389IB.

# II. EXPERIMENT DESCRIPTION

The Power Burst Facility consists of an open tank reactor vessel, a driver core region with an active fuel length of 0.914 m, and a central flux trap region containing an in-pile tube (IPT), with a loop coolant system capable of providing an environment of nominal light water reactor system conditions. The reentrant IPT, which encloses the test space, has inlet and outlet connections for loop coolant flow located at its upper end above the driver core. The coolant enters the top of the IPT and is directed downward on the outside of a flow tube which surrounds the test assembly. At the bottom of the IPT, the coolant flow reverses direction and flows up through the test assembly to the IPT outlet.

The PBF reactor is a facility capable of simulating, through steady state or transient operation, the environment necessary to evaluate various responses of nuclear fuel rods under postulated accident conditions. Test PCM-1 was designed specifically for operation with a molten fuel region within the test rod. The operating conditions were similar to those of previous PCM tests, except for the higher power level selected to provide an upper bound for postulated PCM accidents, and to provide a high probability of molten fuel-coolant interaction upon failure.

This section provides a general description of the experiment configuration and nuclear test conduct. Specific information on the test rod design and instrumentation can be found in Appendix A. The calculational methods for determining average and local test rod power densities during Test PCM-1 are described in Appendix B.

## 1. EXPERIMENT CONFIGURATION

The Test PCM-1 fuel rod design was similar to that of PWR fuel rods except for overall length and fuel enrichment. The fuel pellets were enriched to 20 wt% U-235 and stacked within unirradiated zircaloy-4 cladding to an active fuel column length of 0.914 m. The test rod was backfilled with a mixture of helium and argon gas. The gas composition (77.7% helium and 22.3% argon) was chosen to simulate an end-of-life gas thermal conductivity typical of a commercial PWR fuel rod. The single fuel rod, Rod 201-1, was positioned in a 16.3-mm (inside diameter) zircaloy-4 flow shroud and located in the PBF in-pile flow tube. Nominal design characteristics of the test rod are listed in Table III.

The Test PCM-1 fuel rod and test train assembly are shown in Figure 1. The fuel rod and flow shroud were centered near the axial midplane of the PBF core. The region above the fuel rod and flow shroud, the upper plenum region, contained a particle filter (76-μm mesh size) designed to catch fuel and cladding particles in the event of rod breakup during the test. An orifice plate in the lower assembly was positioned to provide the required flow split between the flow shroud and the area between the shroud and IPT flow tube. The lower plenum region contained a particle filter and catch basket to constrain fuel and cladding particles in the event of test rod breakup.

The Test PCM-1 instrumentation consisted of two categories of instruments; those mounted on the fuel rod and those mounted on the test train assembly. The fuel rod was instrumented for the measurement of the plenum gas pressure, cladding surface temperature, and fuel rod axial elongation. The test train assembly was instrumented for the measurement of coolant pressure, coolant temperature, shroud coolant flow rate, and local neutron flux. The measurements were used to determine the test rod power during the power calibration test phase and for posttest data analysis. The instruments associated with the Test PCM-1 fuel rod are shown relative to the fuel rod and shroud in Figure 1. The instruments associated with the test train are shown in Figure 2. A detailed description of the Test PCM-1 instrumentation is presented in Appendix A.

A fission product detection system (FPDS)[6] was installed for Test PCM-1 to measure the type and quantity of fission products released during rod failure, and to help determine the approximate failure time.

TABLE III

NOMINAL DESIGN CHARACTERISTICS FOR TEST PCM-1
(Rod 201-1)

| | |
|---|---|
| **Fuel** | |
| Material | $UO_2$ sintered pellets |
| Pellet outside diameter | 9.30 mm |
| Pellet length | 15.1 mm |
| Pellet enrichment | 20 wt% U-235 |
| Density | 93% of theoretical |
| Fuel stack length | 0.914 m |
| End configuration | Dished |
| **Cladding** | |
| Material | Zircaloy-4 tubing |
| Tube outside diameter | 10.72 mm |
| Tube inside diameter | 9.50 mm |
| **Fuel Rod** | |
| Filler gas | 77.7% helium - 22.3% argon |
| Fill gas volume | 9.68 $cm^3$ |
| Initial gas pressure | 2.58 MPa |
| Diametral gap | 0.2 mm |
| Plenum length | 50.8 mm |

The detectors were installed downstream of the experiment loop with a sample line tapping the test loop close to the in-pile tube outlet and transporting the loop coolant to a shielded detector enclosure. A schematic representation of the detectors and related electronics is shown in Figure 3.

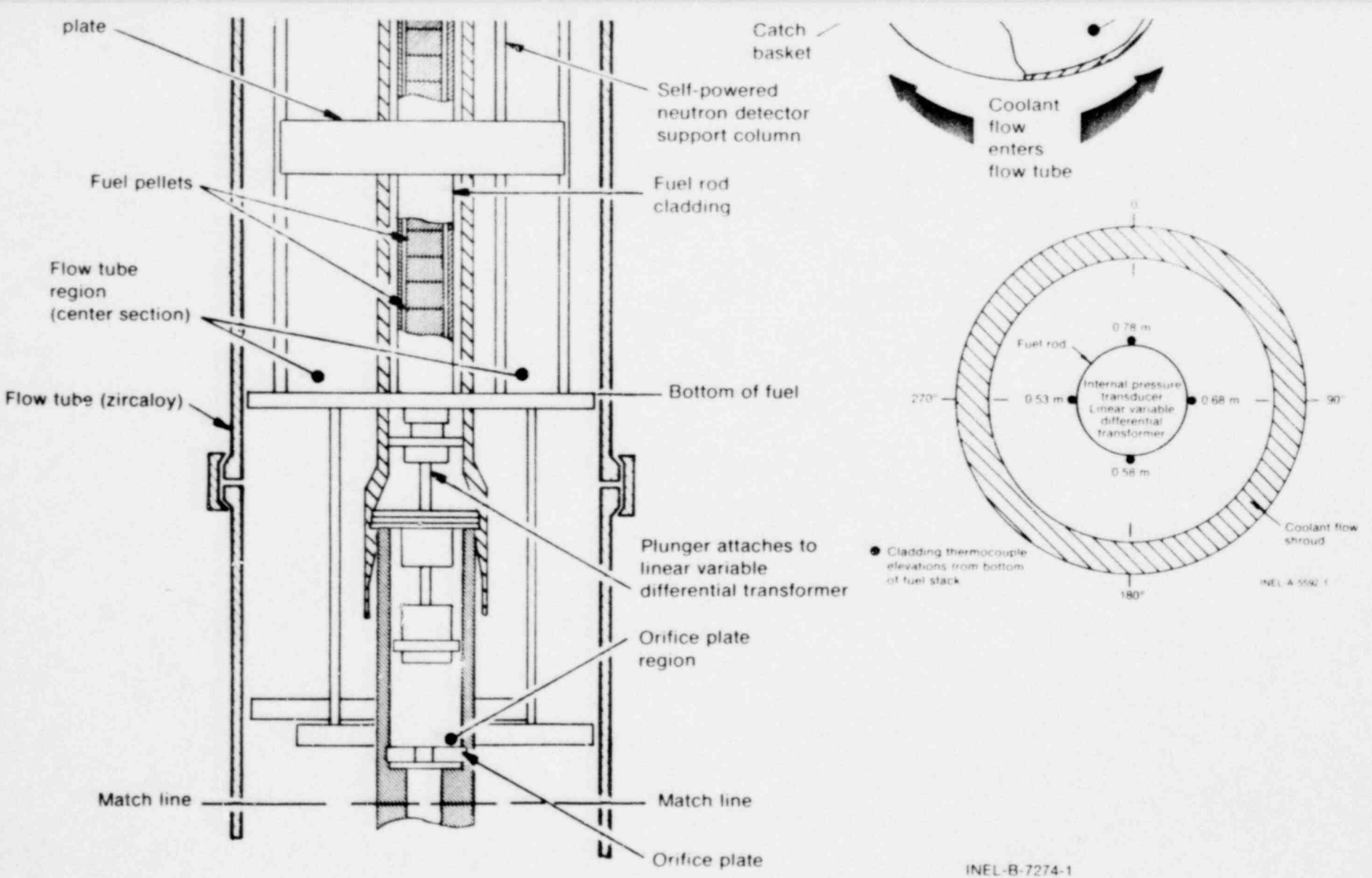


1070 161

**Fig. 1. Test PCM-1 fuel rod and test train assembly.**

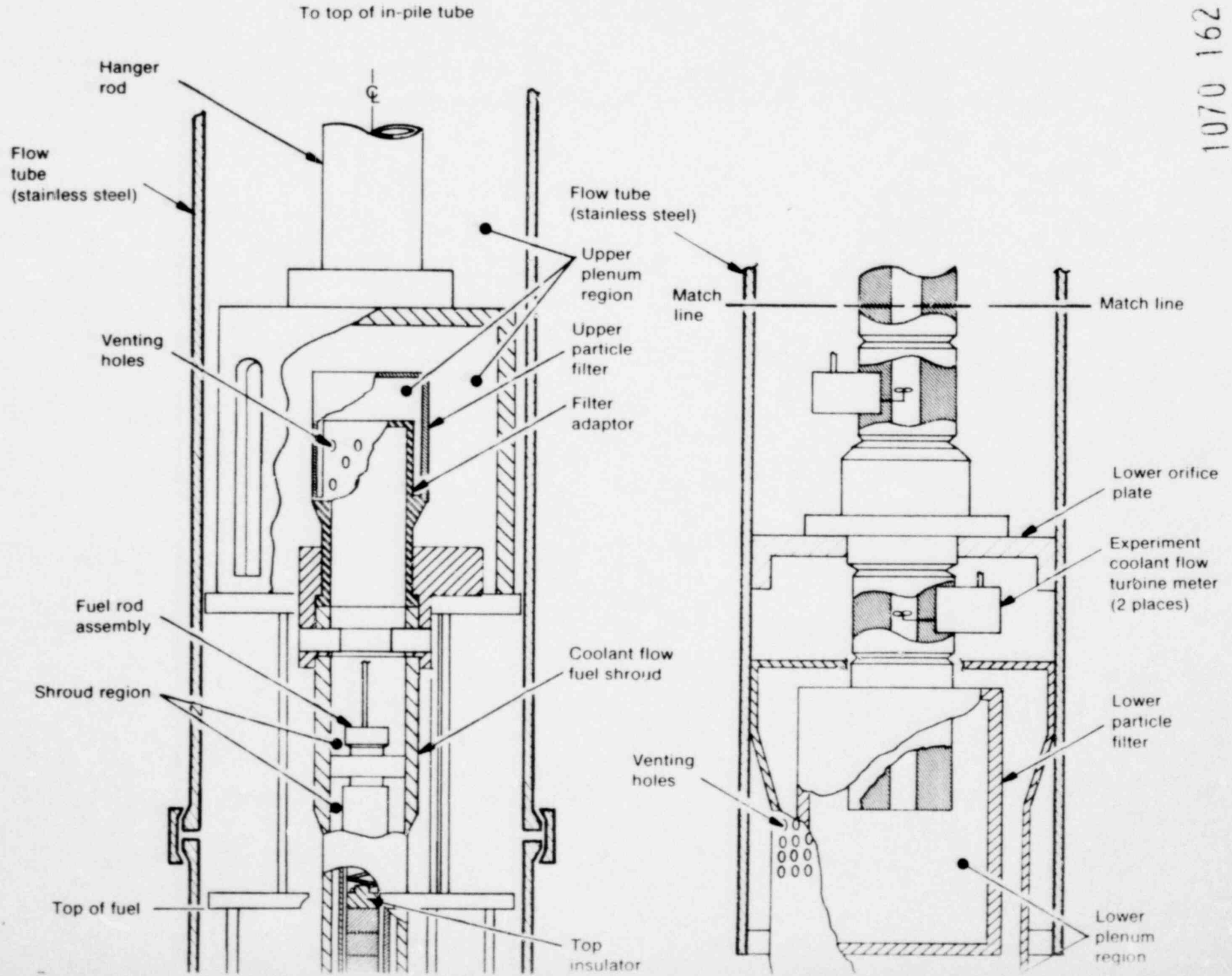
To top of in-pile tube
Hanger rod
Flow tube (stainless steel)
Venting holes
Fuel rod assembly
Shroud region
Top of fuel
Upper plenum region
Upper particle filter
Filter adaptor
Coolant flow fuel shroud
Top insulator
Flow tube (stainless steel)
Match line
Match line
Lower orifice plate
Experiment coolant flow turbine meter (2 places)
Lower particle filter
Venting holes
Lower plenum region

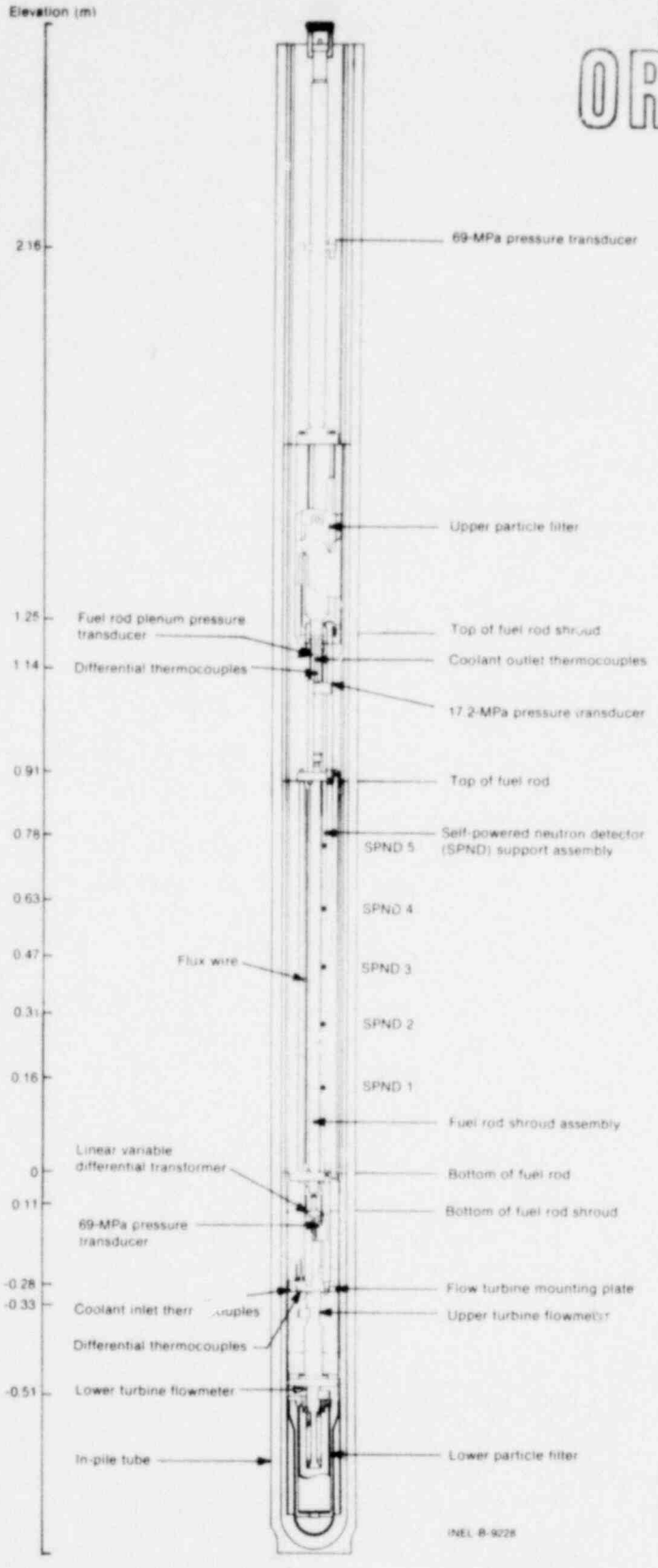


**Fig. 2. Test PCM-1 test train assembly with instrumentation.**

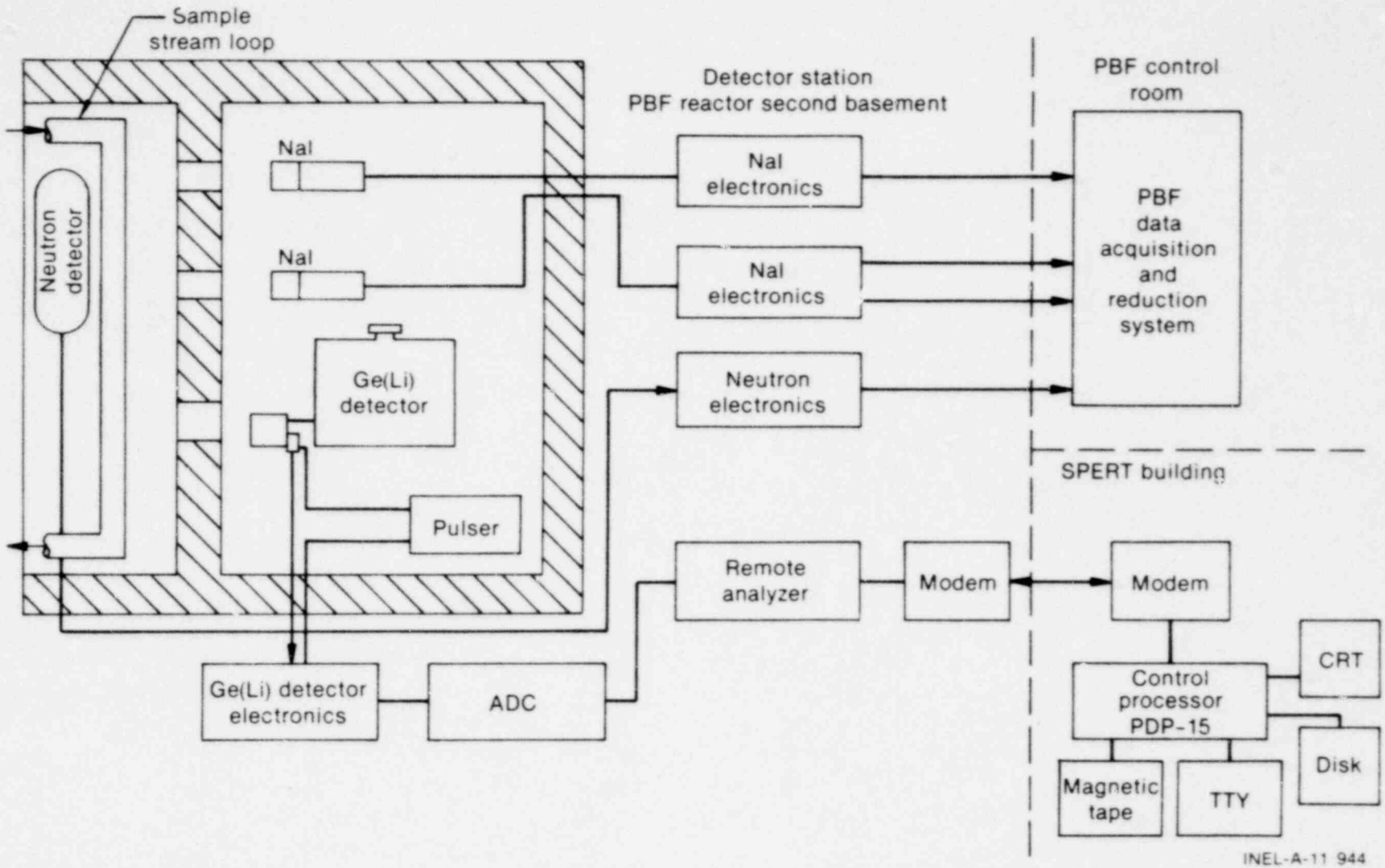


**Fig. 3. Schematic of the fission product detection system instrumentation.**

## 2. TEST CONDUCT

Nuclear operation during Test PCM-1 included (a) a power calibration period during which the test rod power density with respect to self-powered neutron detector (SPND) current was determined; (b) a preconditioning period which caused fuel pellet cracking, accumulation of a fission product inventory, and aging of the cladding surface; and (c) film boiling operation, during which the fuel rod was operated in stable film boiling until failure, and for approximately 7 minutes at full power following failure. Figure 4 shows the reactor core power, test rod peak power density, coolant inlet temperature, and shroud coolant mass flux as functions of time for the entire test. A summary of the test rod powers and thermal-hydraulic conditions during each test phase is presented in Table IV. The three test phases are summarized in the following subsections.

### 2.1 Power Calibration

The purpose of the power calibration test phase was to relate test rod power density determined from a thermal-hydraulic energy balance to self-powered neutron detector (SPND) current. A regression of test rod power and SPND current was used to estimate rod power densities when two-phase outlet coolant conditions were encountered.

The power calibration was accomplished by performing a calorimetric heat balance using the coolant inlet temperature, shroud coolant temperature increase, coolant system pressure, and shroud coolant flow rate. The rod powers were determined at several core power levels at nominal coolant conditions of 15.3 MPa pressure and 600 K inlet temperature. Results from the power calibration are summarized in Table IV.

### 2.2 Preconditioning

The preconditioning phase of the experiment served several purposes. First, the test rod preconditioning provided an operating history sufficient to cause fuel pellet cracking and relocation. Second, the preconditioning "aged" the cladding, thus reducing the possibility of premature DNB occurrence due to outgassing[7]. Third, the preconditioning period served to establish a fission product inventory within the test rod which allowed detection of rod failure as well as the approximate time of the failure by the FPDS.

### 2.3 DNB Testing

The purpose of the DNB test phase was to provide information on the behavior and failure mode of a PWR-type fuel rod subjected to high power operation in the film boiling heat transfer regime. Film boiling was initiated by rapidly increasing test rod peak power from a steady state value of 39 kW/m to 69 kW/m on a ramp of 20 kW/m per minute. The power was held constant for 180 s, and then adjusted to a peak power of 77.8 kW/m. The peak power was attained approximately 350 s after initiation of the transient. The test rod power was held at the adjusted power for approximately 5 minutes[a] following positive indication of cladding failure. The reactor was then scrammed, with subsequent termination of film boiling on the test rod.



a. The rod was actually in high temperature film boiling for slightly over 7 minutes following rod failure, but there was a delay time of 118 s between failure and detection of failure.

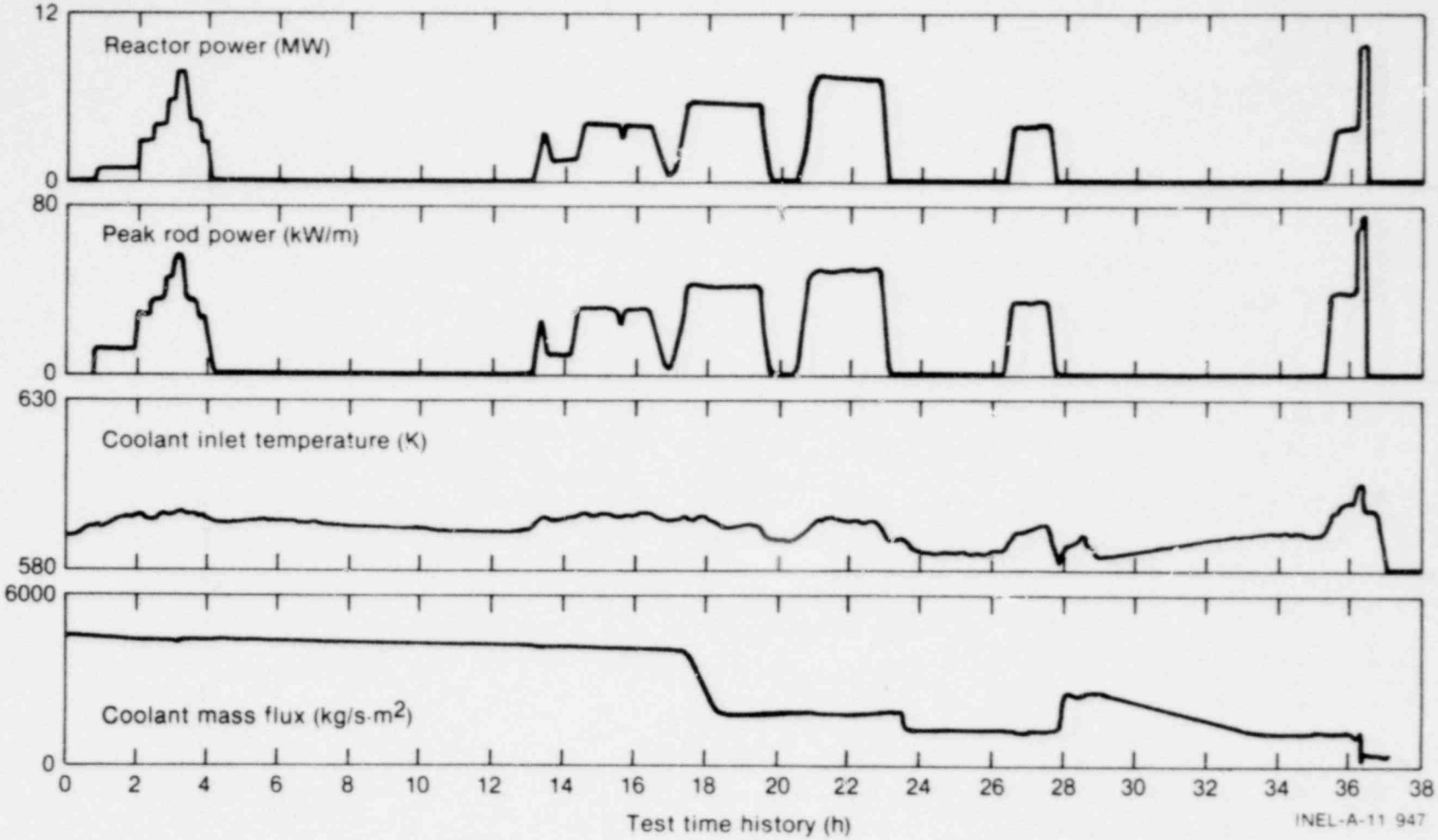


**Fig. 4. Reactor power, test rod peak power, coolant inlet temperature, and through coolant mass flux histories for the power calibration, preconditioning, and DNB test phases.**

## TABLE IV

### SUMMARY OF THERMAL-HYDRAULIC CONDITIONS AND ROD POWERS FOR THE TEST PCM-1 POWER CALIBRATION, PRECONDITIONING, AND DNB TEST PHASES

| | Indicated Reactor Power (MW) | Test Rod Peak Power[a,b] (kW/m) | Test Rod Average Power[a] (kW/m) | Coolant Mass Flux ($kg/s \cdot m^2$) | Inlet Temperature (K) | Coolant ΔT (K) | System Pressure (MPa) |
|---|---|---|---|---|---|---|---|
| Power Calibration Phase | ~0.1 | 0.27 | 0.20 | 4480 | 591 | 0.21 | 15.34 |
| | 2.0 | 12.32 | 9.03 | 4416 | 594 | 2.43 | 15.38 |
| | 4.5 | 28.26 | 20.78 | 4396 | 596 | 5.44 | 15.39 |
| | 6.0 | 35.91 | 26.31 | 4403 | 595 | 6.87 | 15.35 |
| | 8.0 | 46.07 | 33.75 | 4361 | 596 | 8.74 | 15.31 |
| | 10.0 | 57.15 | 41.87 | 4313 | 597 | 10.76 | 15.32 |
| | 6.0 | 36.56 | 26.79 | 4412 | 596 | 6.94 | 15.31 |
| | 4.5 | 27.49 | 20.14 | 4401 | 595 | 5.30 | 15.29 |
| | ~0.1 | 0.28 | 0.21 | 4417 | 594 | 0.15 | 15.31 |
| Preconditioning Phase | ~0.1 | 0.38 | 0.28 | 4272 | 591 | 0.08 | 15.14 |
| | 5.0 | 27.30 | 20.00 | 4400 | 595 | 5.30 | 15.30 |
| | 1.5 | 10.30 | 7.55 | 4174 | 595 | 2.12 | 15.15 |
| | 5.1 | 31.68 | 23.21 | 4088 | 596 | 6.43 | 15.17 |
| | ~0.1 | 3.41 | 2.50 | 4080 | 595 | 0.72 | 15.23 |
| | 7.0 | 42.75 | 31.32 | 3202 | 595 | 11.02 | 15.20 |
| | 7.0 | 42.36 | 31.04 | 1797 | 594 | c | 15.28 |
| | 0.1 | 0.45 | 0.33 | 1840 | 589 | 0.21 | 15.24 |
| | 9.0 | 50.13 | 36.72 | 1796 | 595 | c | 15.22 |
| | ~0.1 | 0.22 | 0.17 | 1501 | 587 | 0.14 | 15.22 |
| | 6.0 | 35.77 | 26.21 | 1232 | 591 | c | 15.43 |
| | ~0.1 | 0.35 | 0.26 | 2253 | 587 | 0.15 | 15.38 |
| DNB Phase | ~0.1 | 0.51 | 0.38 | 1170 | 591 | 0.23 | 15.18 |
| | 6.4 | 38.60 | 28.28 | 1188 | 597 | c | 15.22 |
| | 11.5 | 69.34 | 50.80 | 1110 | 603 | c | 15.27 |
| | 12.6 | 75.62 | 55.40 | 1052 | 605 | c | 15.21 |
| | 12.8 | 76.57 | 56.1 | 980 | 606 | c | 15.25 |
| | 13.0 | 77.80 | 57.0 | 1087 | 605 | c | 15.25 |

a. Rod power was determined by regression of the SPNDs with subcooled thermal energy balance data.

b. Test rod peak power is based on a peak-to-average ratio of 1.365 obtained from Co-Al flux wire data.

c. ΔT measurement unreliable due to saturated outlet coolant conditions.

# III. FUEL ROD BEHAVIOR DURING FILM BOILING OPERATION

The primary objectives of Test PCM-1 were to evaluate the behavior of a fuel rod operated under high temperature film boiling conditions for a time beyond cladding failure, with large local regions of molten fuel providing the potential for energetic molten fuel-coolant interaction upon failure. This section presents the fuel rod behavior results as interpretted from the in-pile instrumentation and posttest examination.

## 1. FUEL ROD BEHAVIOR RESULTS OBTAINED FROM IN-PILE INSTRUMENTATION

The behavior of a fuel rod operating in the film boiling heat transfer regime generally must be inferred from a combination of in-pile temperature, pressure, flow, and mechanical deformation measurements, calculational techniques, and posttest information. The analyses contained in this section are based on the available on-line instrumentation responses and FRAP-T4 computer code calculations. The cladding temperature history, time to fuel rod failure, mechanism of failure, and the measurable consequences of failure are inferred from these analyses.

The power and coolant conditions during the DNB phase of Test PCM-1 are shown in Figure 5. The system pressure was nominally 15.2 MPa during the entire experiment. The transient was initiated by rapidly increasing the rod peak power from 39 to 69 kW/m at a rate of 20 kW/m per minute. The power and coolant conditions were held relatively constant for 180 s; the power was then adjusted to 77.8 kW/m for the remainder of the DNB testing phase. Zero time on Figure 5 corresponds to the start of the Test PCM-1 power ramp, and is used as the reference time throughout this report. The reactor power was rapidly decreased 920 s after the initial power ramp to terminate the experiment.

Fuel rod behavior during Test PCM-1 was evaluated using four primary measurements; cladding surface temperature, cladding elongation, loop fission product activity level, and rod internal pressure. The cladding temperature measurements during the DNB test phase are shown for three of the measurement elevations in Figure 6. The instrument located at the 0.53-m elevation (measured from the bottom of the fuel

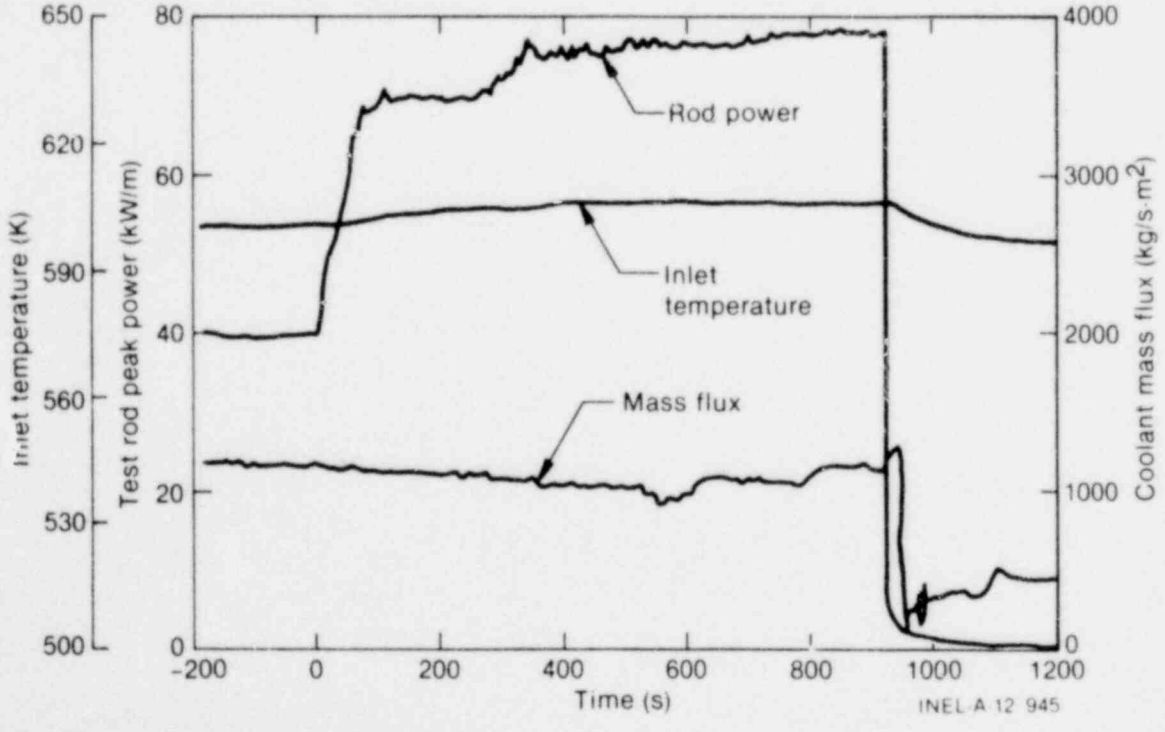


**Fig. 5. Coolant conditions and test rod peak power generation for the DNB phase of Test PCM-1.**

1070 168

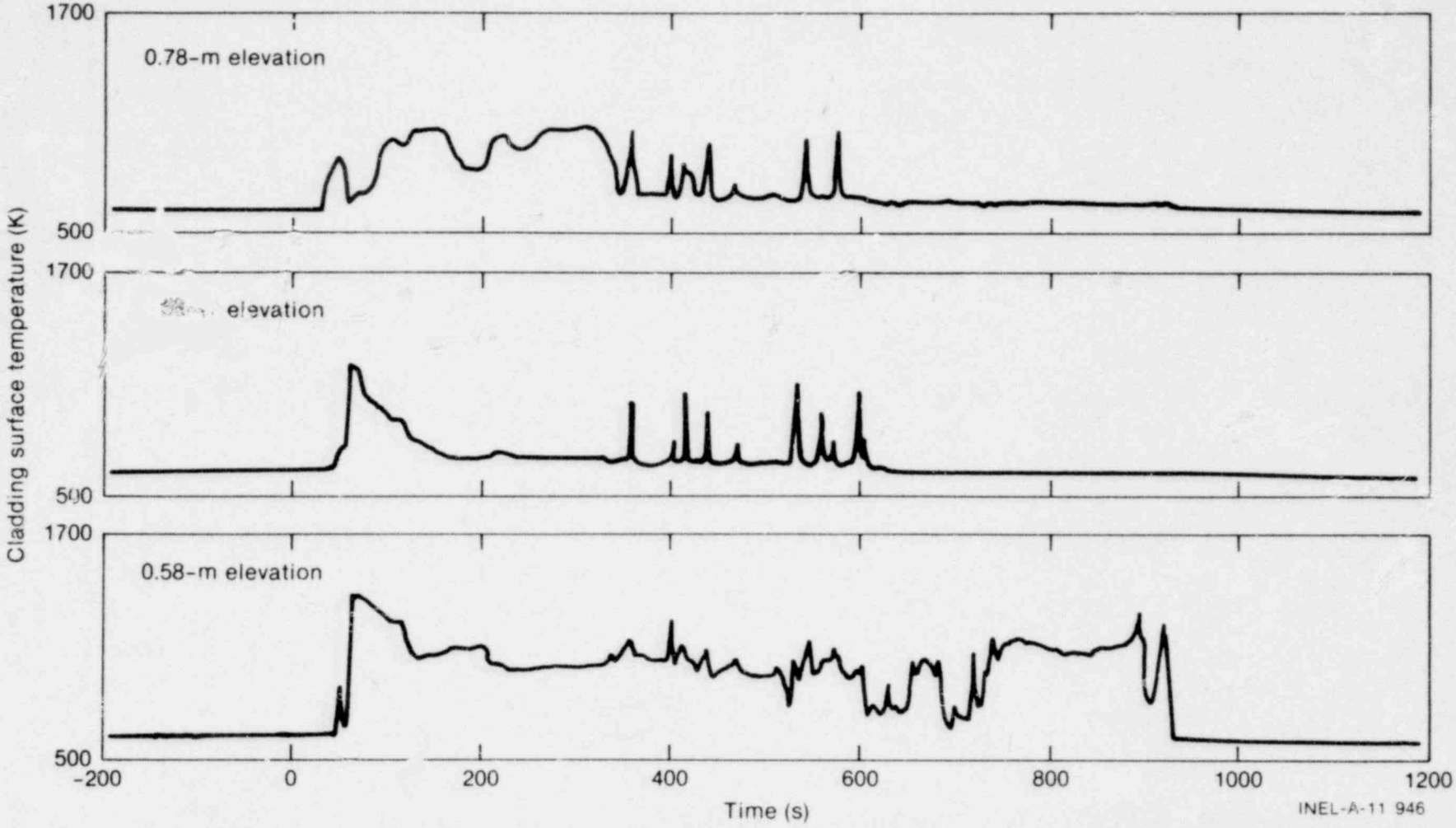


**Fig. 6. Indicated cladding surface temperature response for the 0.58-, 0.68-, and 0.78-m elevations for the DNB phase of Test PCM-1.**

stalk) failed early in the power transient and is not included in Figure 6. A limited amount of information was obtained from the cladding temperature measurements due to the increasingly erratic behavior of the thermocouples during film boiling operation. The definitive cause of the erratic behavior could not be ascertained, but was probably due to a combination of high cladding temperatures, cladding oxide buildup under the thermocouples, and unstable film conditions on the protruding thermocouples.

### 1.1 Onset and Propagation of Film Boiling

The axial progression of film boiling was determined from the cladding surface temperature measurements. The first indication of the degraded heat transfer conditions occurred at the 0.78-m elevation, 24 s after the Test PCM-1 power ramp was initiated. The lower elevations sequentially responded to the film boiling conditions. Table V lists the time and conditions of first indication of film boiling for each of the cladding temperature measurements and the cladding elongation measurement. The response of the cladding thermocouple at the 0.53-m elevation is included in Table V even though the device failed shortly after DNB indication. The Test PCM-1 conditions at the first indication of film boiling are shown in Figure 7. For comparision, previous PCM test data and the Test PCM-1 data at the onset of film boiling are also shown in Figure 7.

TABLE V

FILM BOILING INDICATIONS AND CONDITIONS FOR TEST PCM-1

| | Cladding Temperature | | | | |
|---|---|---|---|---|---|
| | 0.78 m | 0.68 m | 0.58 m | 0.53 m | Cladding Elongation |
| Time after power ramp initiation(s) | 24 | 39 | 44 | 45 | 39 |
| Test rod peak power (kW/m) | 51.9 | 56.0 | 59.5 | 59.7 | 56.0 |
| Local rod power (kW/m) | 28.1 | 42.1 | 53.5 | 56.2 | -- |
| Shroud coolant mass flux (kg/s.m2) | 1135 | 1140 | 1143 | 1143 | 1140 |
| Coolant inlet temperature (K) | 599 | 600 | 600 | 600 | 600 |

### 1.2 Cladding Temperature Estimates

The cladding peak temperature history during film boiling operation was estimated using FRAP-T4 computer code calculations in conjunction with local cladding temperature measurements. The increasingly erratic indications by the cladding surface thermocouples preclude using the values after approximately 150 s. The maximum measured cladding temperatures in the first 150 s were corrected for the estimated amount[a] of fin cooling[8,9] and compared with the FRAP-T4 estimates. The comparison, shown

a. The magnitude of fin cooling is very temperature dependent. A value of 200 K was estimated at the highest measured temperatures.

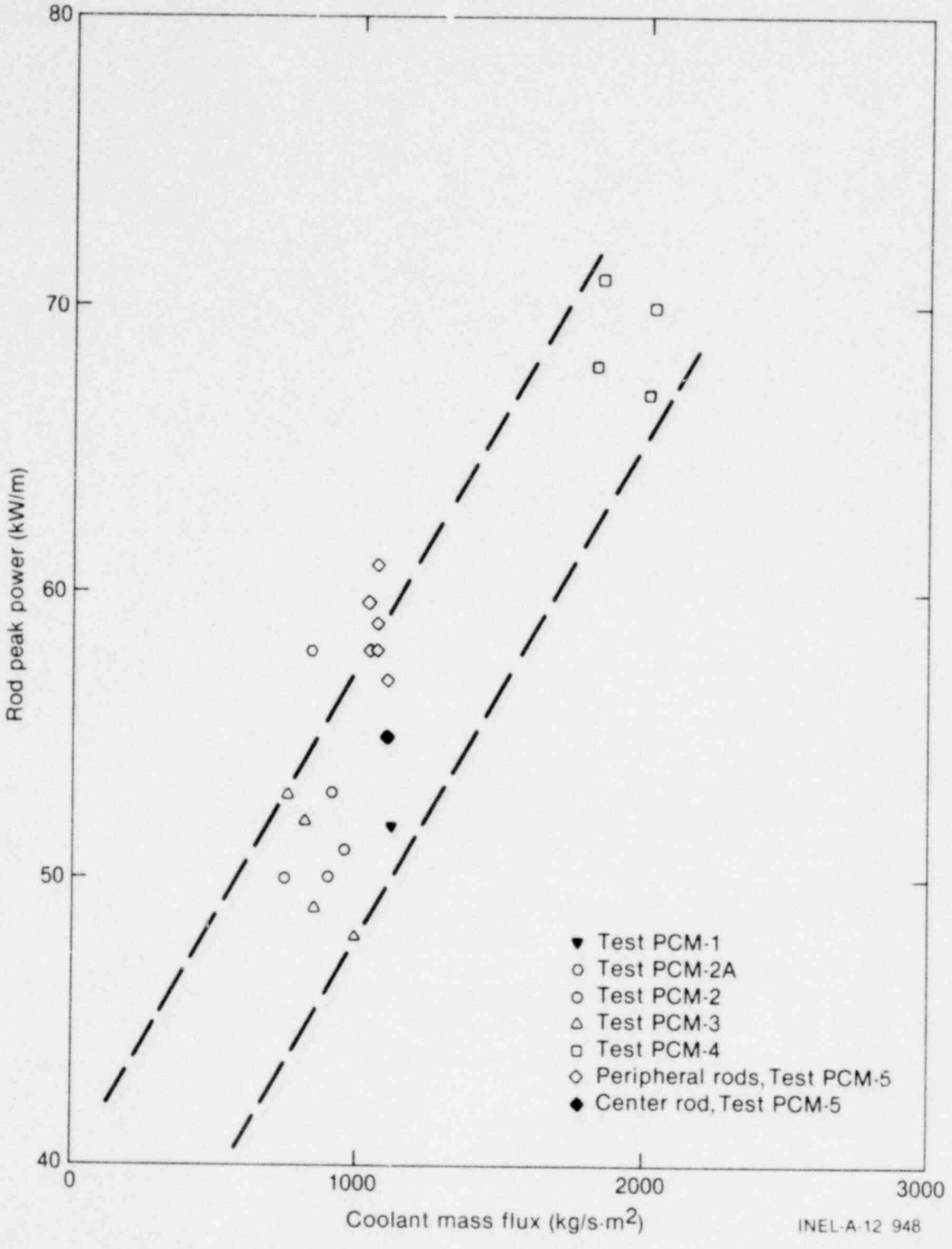


**Fig. 7. Comparison of the conditions at first indication of film boiling for the PCM Test Series.**

in Figure 8 for the three axial measurement elevations, indicates good agreement between the measured and calculated cladding peak temperatures. The cladding temperature estimates obtained from metallurgical examinations (discussed in Section III-2) are also shown in Figure 8 and consistency with the on-line measurements and calculated temperatures is illustrated. The agreement between the measured and calculated cladding peak temperatures provided confidence that the FRAP-T4 calculated temperature

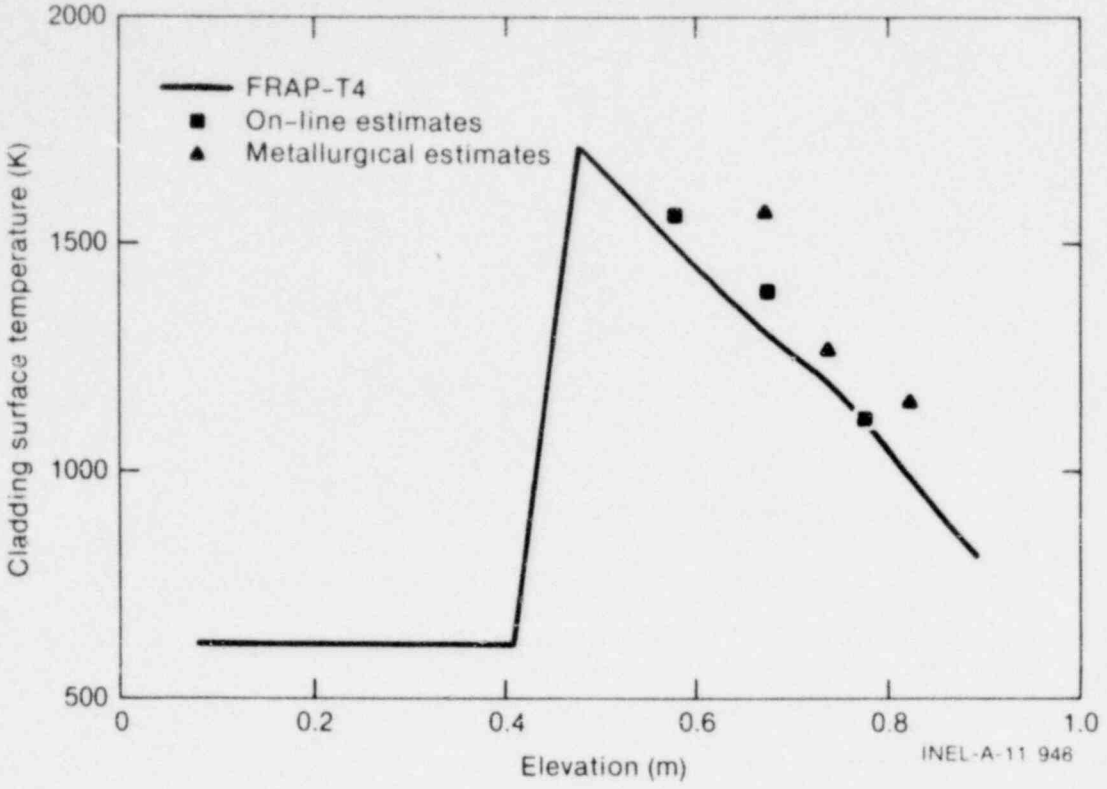


**Fig. 8. Axial cladding surface temperature profile calculated by FRAP-T4 and measured cladding peak temperatures for the initial film boiling period.**

history could be used as the "best estimate" cladding temperature history. The calculated cladding maximum temperature history, referenced to the start of the Test PCM-1 power ramp, is presented in Figure 9. A cladding peak temperature of 1875 K was calculated during the DNB test phase.

### 1.3 Rod Failure

The at-power rod failure time was determined from the FPDS loop gamma activity measurement and the cladding elongation response. The cladding elongation response and a measurement of the loop gamma activity are shown for the DNB test phase in Figure 10. The rapid change in cladding elongation 39 s after the initial power ramp corresponds to the rapid length change associated with film boiling conditions on the fuel rod. The cladding length remained fairly constant (within 0.25 mm) from 125 s to the power adjustment at 283 s, indicating stable film boiling along a relatively constant axial extent of the Test PCM-1 fuel rod. Comparison with a similar design single-rod experiment[10] indicates that the 5.4-mm increase in rod length during the initial portion of the DNB test phase corresponds to a film boiling axial extent of approximately 0.4 m.

The fission product detection system instrumentation responded to large increases in the loop gamma activity at two times during the DNB test phase. The first increase, corresponding to the initial fuel rod failure, occurred 637 s after the start of the power ramp. The second large activity detection occurred approximately 105 s after reactor scram (1025 s referenced to the start of the power ramp) and corresponds to gross breakup of the test rod following rewet. Previous testing of fuel rods having experienced severe PCM conditions has shown that highly embrittled test rods (due to cladding oxidation) will fail following rewet from film boiling conditions[11]. This observation and the extreme test conditions allowed determination of the delay time between the release of fission products at the failure location and the downstream detection (the transport delay time) by using the delay between the reactor shutdown and the ensuing FPDS

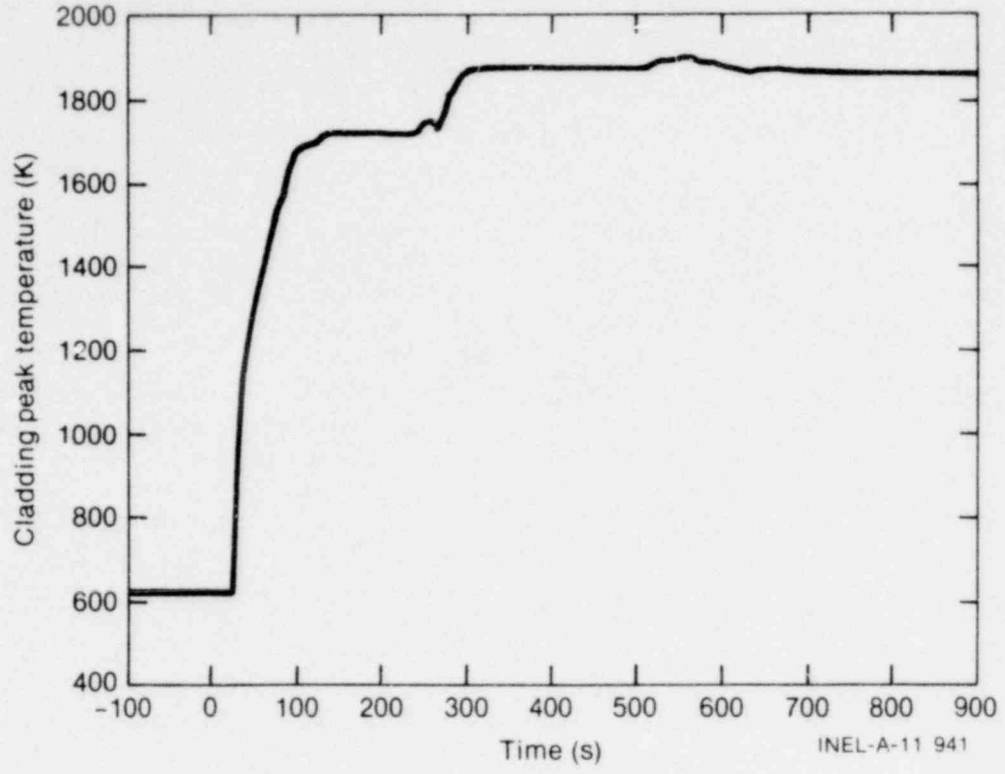


**Fig. 9. FRAP-T4 calculated peak temperature history during the DNB phase of Test PCM-1.**

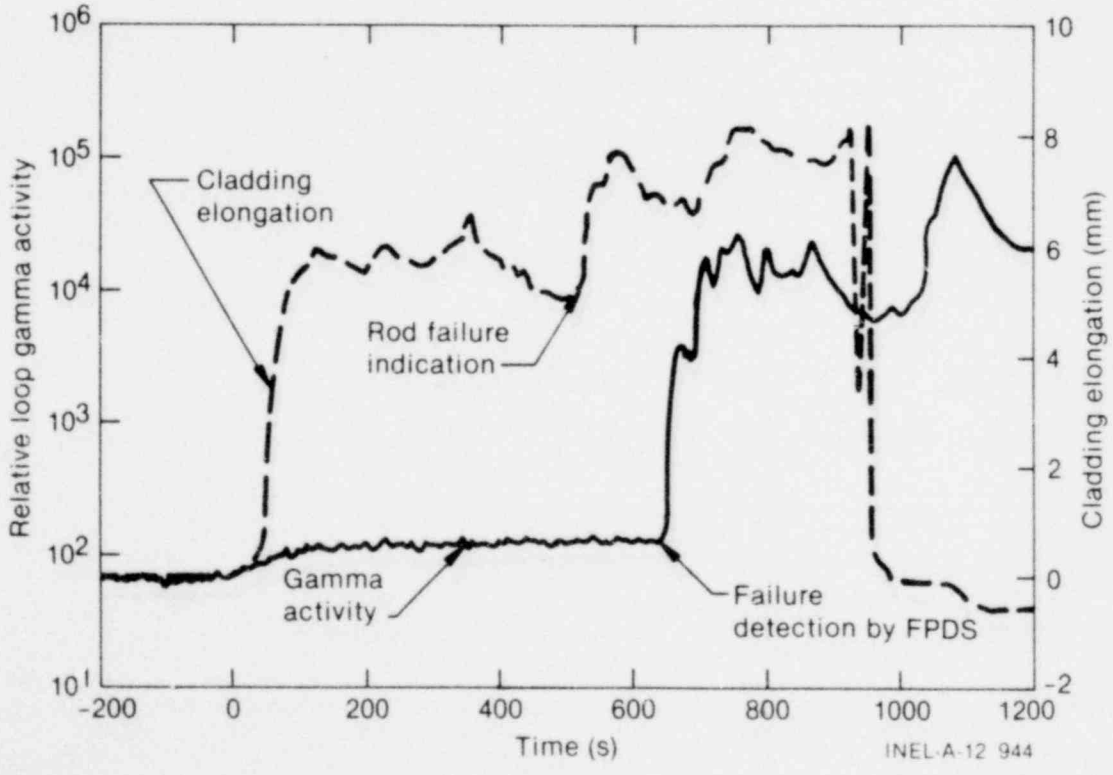


**Fig. 10. Cladding elongation and fission product detection system gamma detector response for the DNB phase of Test PCM-1.**

response. The delay time was found to be 105 $^{+6}_{-45}$ s. The uncertainties in the delay time stem from the interpretation of the gamma detector response to the failure and the estimated rewet time of the fuel rod.

The at-power failure time was determined through use of the first gamma increase detected in the loop (at 637 s) and the shutdown delay time. The relative flow rates during the postshutdown detection period and a comparable time preceding the initial detection of failure were used to adjust the failure delay time. The delay time from the test space to the FPDS detectors was found to be 118 s, resulting in a best-estimate initial rod failure time of 519 s. The best estimate of the time of failure corresponds to within 1 s with the rapid cladding elongation increase at 520 s, suggesting that positive indication of the fuel rod failure was given by the cladding elongation measurement.

The magnitude of the cladding length change at 520 s (2.7 mm) implies that the initial failure of the fuel rod was not a localized failure, but rather a complete separation of the rod. The axial location of the rod fracture cannot be precisely determined from the cladding elongation response due to large uncertainties in the spring constant of the elongation sensor [linear variable differential transformer (LVDT)], the equilibrium positioning of the sensor, and the mass of some fuel rod assembly components (end caps, insulator pellets, etc.). On the basis of nominal LVDT spring constant data, the observed deflection (2.7 mm) would have been caused by the weight of a fuel rod segment 150 mm in length. However, on the basis of postirradiation examination results, the rod fractured at a much higher elevation.

The shroud-to-loop flow ratio changed after the initial rod failure (520 s), indicating a change in geometry within the coolant flow shroud. Figure 11 shows the ratio of the shroud flow to the overall loop flow during the DNB test phase. The ratio, which is an indication of the intrashroud flow resistance, decreased at approximately 520 s, indicating a higher resistance within the flow shroud following rod failure. An additional increase in the shroud resistance was indicated following rewet of the rod (at approximately 930 s) which resulted in an 80% reduction of the shroud flow.

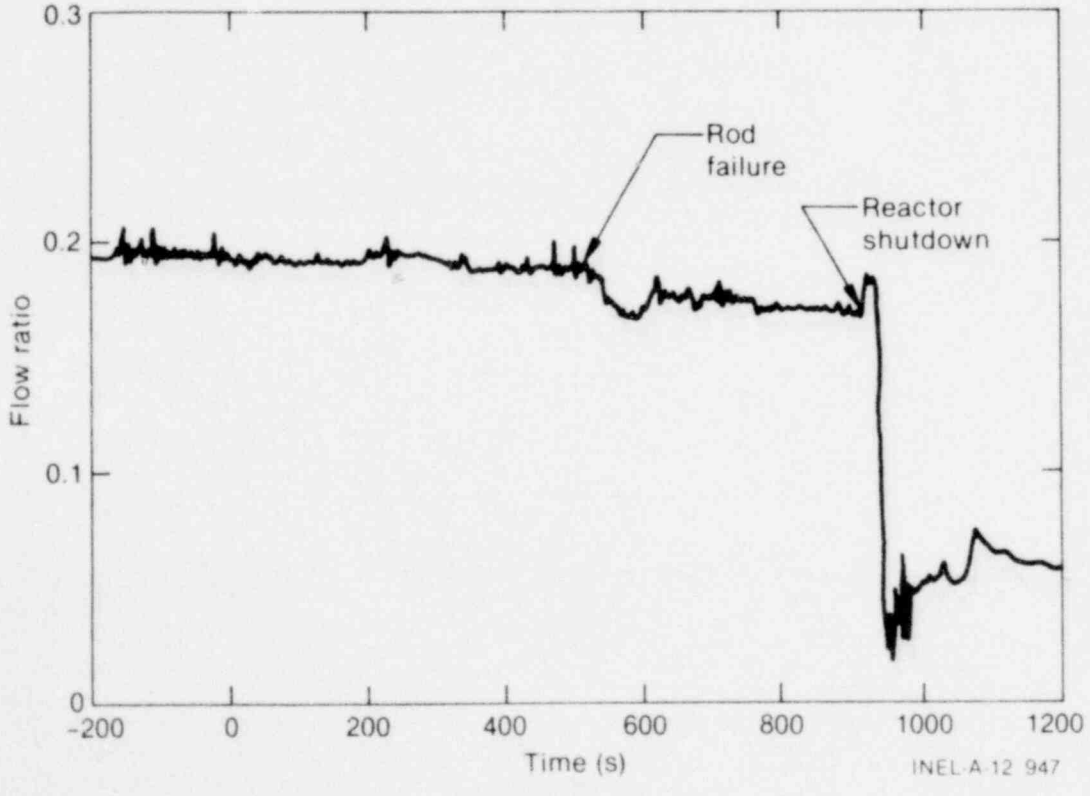


**Fig. 11. Ratio of shroud-to-loop flow rate during the DNB phase of Test PCM-1.**

The failure of the test rod at 520 s was not detected by the internal pressure measurement in the upper rod plenum region. The rod internal pressure response, shown in Figure 12 for the DNB test phase, did not indicate system pressure until the reactor was scrammed and the test rod rewet at approximately 930 s. The large difference between the coolant system pressure and the rod internal pressure (approximately 6.5 MPa) caused collapse of the high temperature cladding onto the fuel stack, impeding gas flow from the failure location to the fuel rod plenum during operation. Cooling of the rod following rewet resulted in a communication path between the failure region and the fuel rod upper plenum. The coolant system pressure, also shown in Figure 12, showed no response which would be considered a result of violent molten fuel-coolant interaction, either immediately following the rod failure or during the continued test operation.

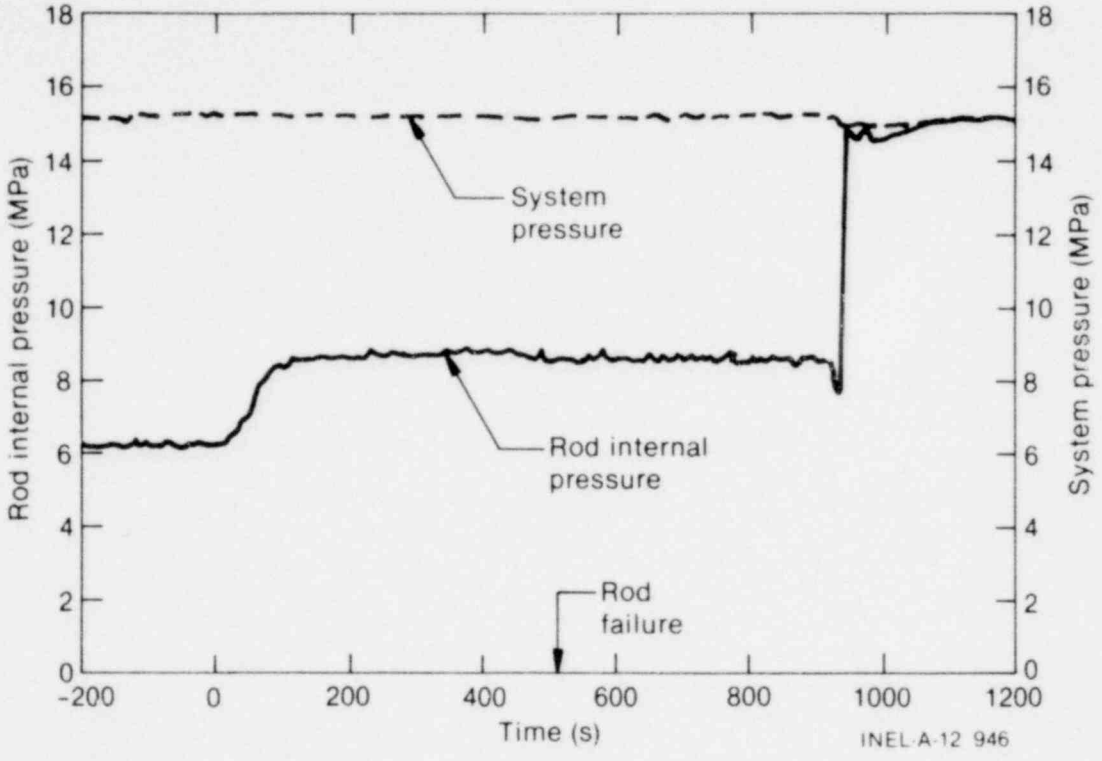


**Fig. 12. Rod internal pressure and coolant system pressure for the DNB phase of Test PCM-1.**

### 1.4 Cladding Embrittlement

Calculation of the degree of cladding oxidation and embrittlement at the time of rod failure was made possible by determination of the rod failure time and the cladding peak temperature history (Figure 9). The calculation provides insight into the mechanism of the fuel rod failure.

A modified version of the BUILD5 computer code[a] was used to calculate the extent of external cladding oxidation for the Test PCM-1 temperature history. The Cathcart oxidation kinetics correlations[15] are used within the code to calculate the buildup of oxide ($ZrO_2$) and oxygen-stabilized alpha-zircaloy on the outside surface of the cladding. Since the calculated cladding peak temperatures (1875 K) during the high power operation were above the published upper limit of the correlation (1773 K), the upper limit of the oxidation kinetics correlation was used for the analysis. The resulting oxygenation values are, therefore, a

a. The BUILD5 computer code was developed by R. Pawel at the Oak Ridge National Laboratory[12,13]. The modified program is presented in Appendix F of Reference 14.

minimum that would be expected during the test. In addition to the external oxygenation process, an oxygen-stabilized alpha-zircaloy layer is produced on the cladding inner surface due to a zircaloy-$UO_2$ reaction when the high temperature cladding collapses onto the fuel stack. An estimate for the Test PCM-1 internal alpha-zircaloy thickness was obtained using the results of Hoffman and Politis[16].

A high temperature embrittlement criterion was obtained on the basis of extrapolation of published fractional remaining wall thickness (of beta-phase zircaloy) and nil-ductility temperature data[17]. The extrapolation suggested that the nil-ductility point would be achieved at the Test PCM-1 cladding peak temperatures when 100% of the cladding wall was converted to either alpha-zircaloy or $ZrO_2$. The equivalent cladding reacted (ECR)[18] to $ZrO_2$ is a parameter used to relate the zircaloy reaction products to an embrittlement criterion. The extrapolated embrittlement criteria for Test PCM-1 resulted in an ECR value of 24% before failure due to embrittlement would be expected. At the Test PCM-1 fuel rod failure time (520 s), the correlation-limited temperature history resulted in a 21.5% ECR. Since the ECR value was a minimum value for the Test PCM-1 operation due to the temperature limit of the correlation, the mechanism of the initial rod failure was most likely embrittlement caused by nearly complete reaction of the cladding to oxygen-stabilized alpha-zircaloy and $ZrO_2$. The equivalent cladding reacted and its constituent parts are shown in Figure 13. The temperature history (limited by the range of the correlation) for the DNB test phase is also shown in Figure 13.

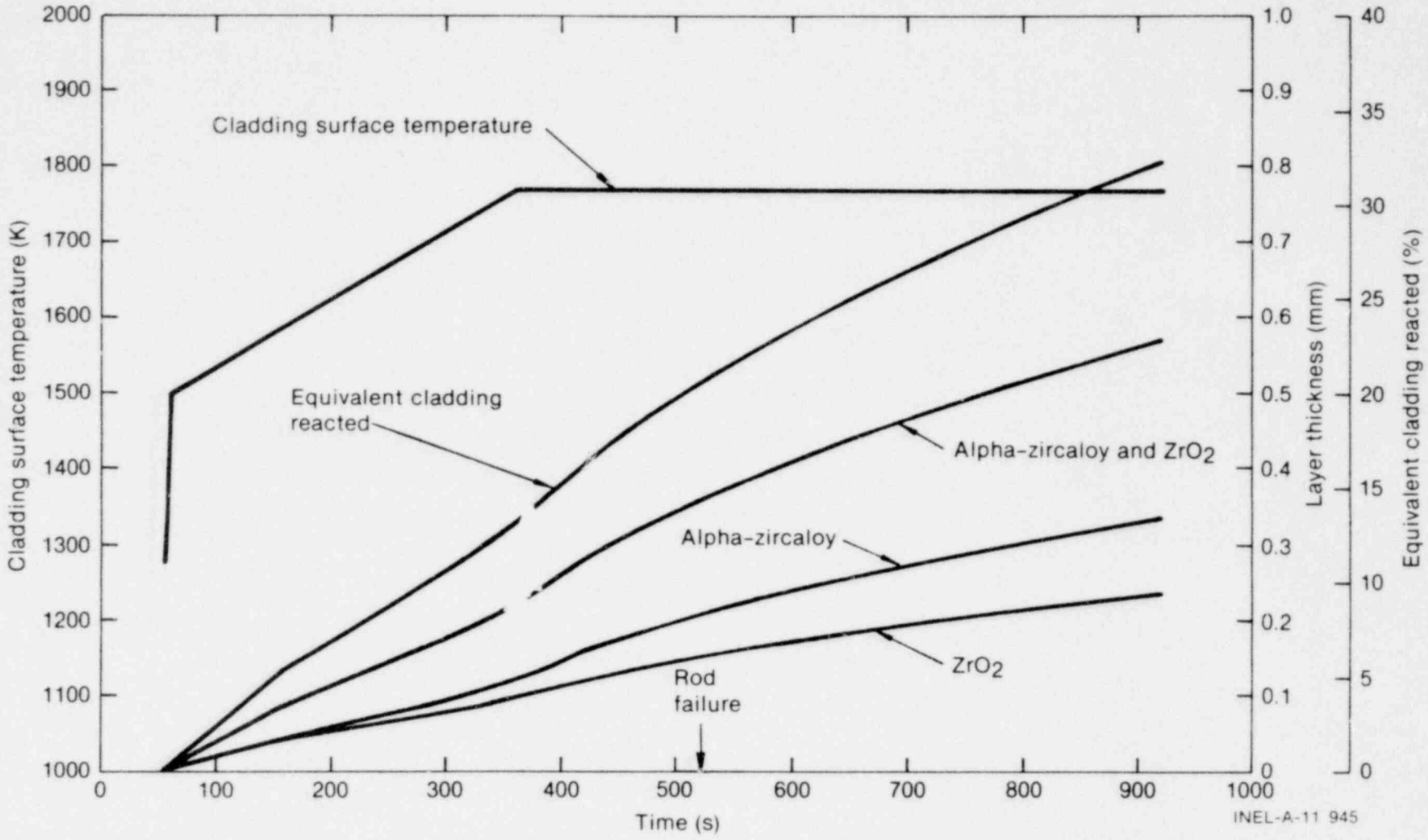


**Fig. 13. One-sided oxide thickness as calculated by BUILD5 on the basis of the estimated time-temperature history for the DNB test phase. Also shown is the percent equivalent cladding reacted as calculated on the basis of the alpha-zircaloy and $ZrO_2$ layer thicknesses.**

## 2. FUEL ROD BEHAVIOR RESULTS OBTAINED FROM POSTTEST EXAMINATION

Posttest examination[4] of the Test PCM-1 rod was conducted to help evaluate the behavior of a fuel rod operated for a significant time following failure, and to determine the consequences of operation. The emphasis of this section is on the interpretation of the posttest examination results relative to the fuel rod behavior, the mechanism of failure, and the consequences of failure.

The Test PCM-1 flow shroud was split longitudinally to allow posttest visual examination of the test rod. Figure 14 illustrates the overall posttest condition of the failed fuel rod. The lower film boiling boundary is indicated by the transition from a dark to light oxide at 0.36 m on the scale of Figure 14 (0.22 m above the bottom of the fuel stack). The distinct transition boundary at the bottom of the film boiling zone has been observed in previous PCM single-rod experiments[8,9]. The more diffuse, upper film boiling boundary was determined from cladding microstructure to be at approximately 1.02 m (0.85 m from the bottom of the fuel stack). [Filings from the shroud splitting process are seen in the lower, enlarged portion of the shroud (0 to 0.1 m) and between 0.79 to 0.80 m on the scale of Figure 14.]

Broken pieces of cladding lying around the bottom end cap (0.12 m) and loose fuel pieces (and missing rod sections) in the high power region of the rod (0.44 to 0.80 m) illustrate the degree of damage incurred by the Test PCM-1 fuel rod. The top intact portion of the fuel rod begins at 0.80 m (0.63 m from the bottom of the fuel stack) and is positioned in its original axial location within the shroud. The bottom section of the rod (below 0.44 m) dropped down in the shroud. A thin, white deposit on the inside surface of the shroud matching a pattern of white oxide on the cladding (0.35 and 0.37 m, respectively) suggests that the bottom portion of the rod dropped down in the shroud during or shortly after power operation.

Several large pieces of cladding were found to be relocated around the top and bottom end caps of the rod. Several of the cladding pieces were examined metallographically and found to be only partially oxidized. The partially oxidized fracture surfaces suggest that the fragments fell into the coolant stream immediately after fracture. On the basis of the extent of oxidation of the intact rod segments, the cladding fragments would have been completely oxidized had they remained on the rod in the high power region. Apparently, when the rod fractured at 520 s, the intrashroud geometry changed sufficiently to cause wetting of some portions of the cladding which had not been completely oxidized. Although some ductility remained at high temperatures, portions of the rewet cladding were sufficiently embrittled to break up.

Additional evidence of cladding breakup during film boiling operation can be seen by comparing the fuel melt radii of those fuel pieces without intact cladding from the high power region of the rod with those pieces which had cladding attached. The fuel pieces with no intact cladding had smaller melt radii than pieces at locations in lower power regions with cladding still intact. After cladding breakup in the high power region, oxidation of the intact cladding at lower power regions continued, insulating the fuel and resulting in higher fuel temperatures. Figure 15 shows the ends of various Test PCM-1 rod pieces and illustrates (by means of the fuel melt radii) the higher fuel temperatures experienced by fuel pieces with the oxidized cladding still attached.

A large portion of the fuel rod disintegrated into pieces smaller than 76 μm (the shroud screen mesh size) and were swept out of the fuel rod assembly by the coolant flow. Twenty-four percent of the original fuel stack mass (34% of the maximum film boiling zone) either dispersed upon contact with the coolant or shattered into pieces small enough to pass through the shroud particle screens. No posttest evidence of energetic molten fuel-coolant interaction was observed.

Rewet of the rod following shutdown caused rod breakup, resulting in an 80% blockage of the shroud coolant flow (as discussed in Section III-1). Posttest examination revealed large cladding pieces at the upper and lower end cap locations, as shown in Figure 16. Additional breakup of the rod upon rewet and relocation of cladding and rod pieces probably caused the observed flow blockage. Fuel pieces were not abundant in the suspected blockage locations.

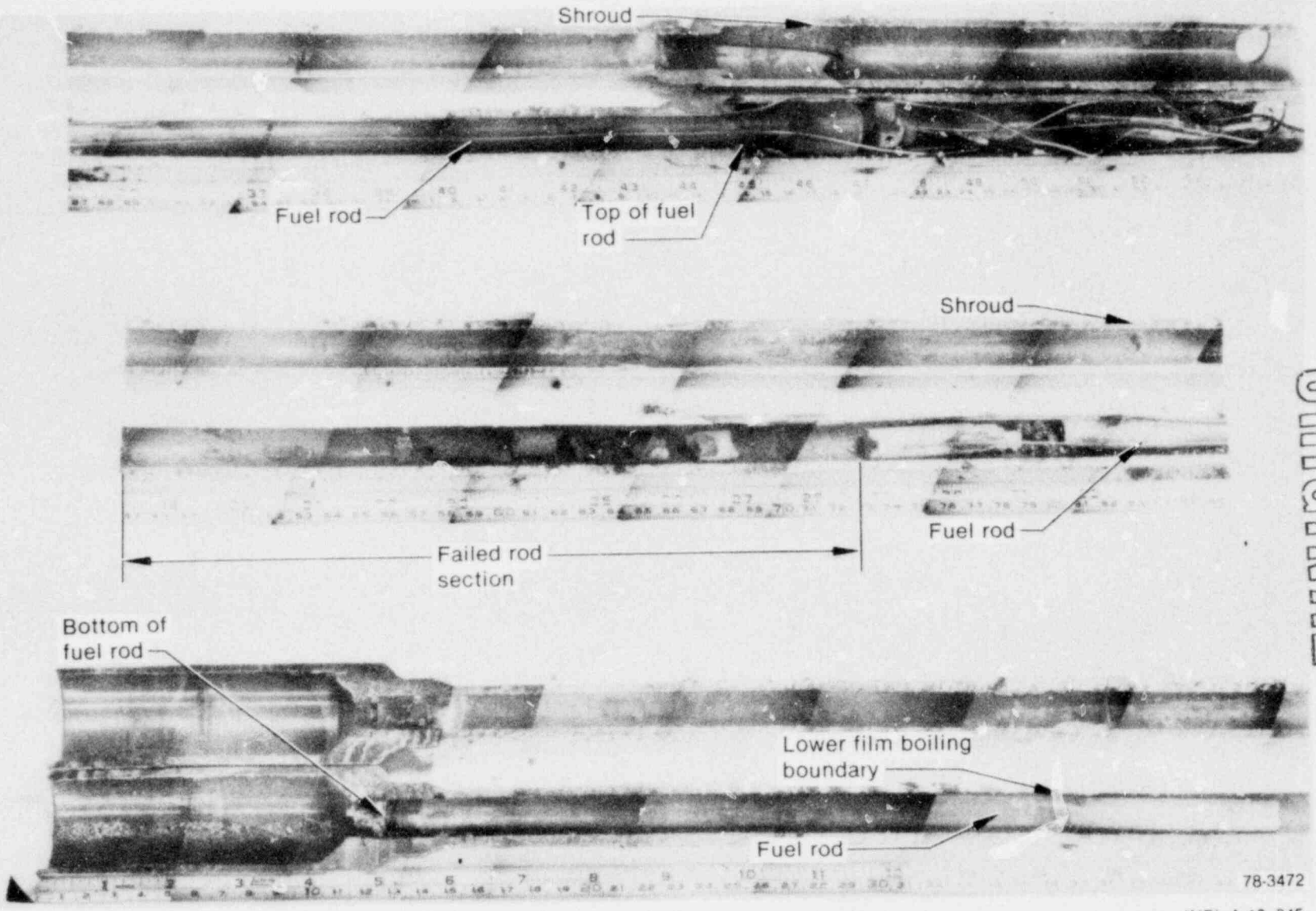


Fig. 14. Overall posttest view of Test PCM-1 fuel rod in opened shroud.

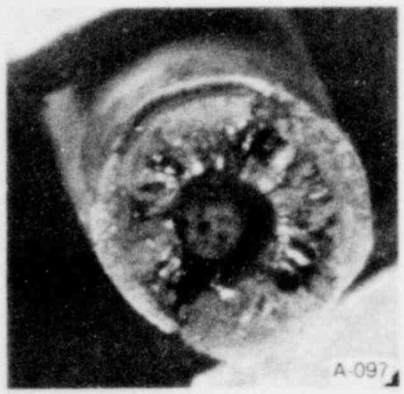


(a) Loose fuel piece with cladding


(b) Loose fuel piece without cladding



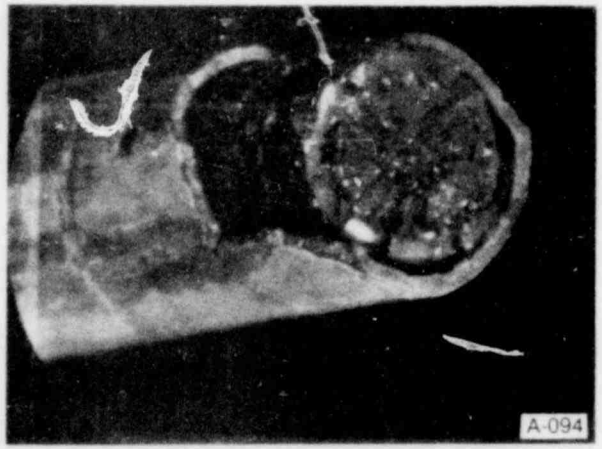


(c) Top end of bottom intact section

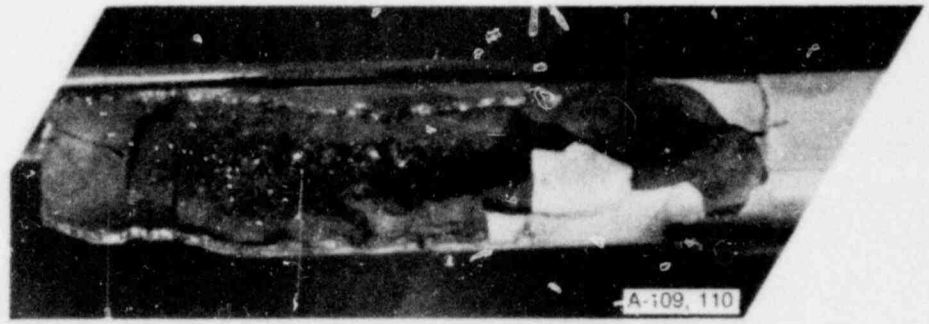


(d) Bottom end of top intact section

INEL-A-13 046

Fig. 15. Test PCM-1 fuel rod segments illustrating the effect of postfailure internal oxide buildup.

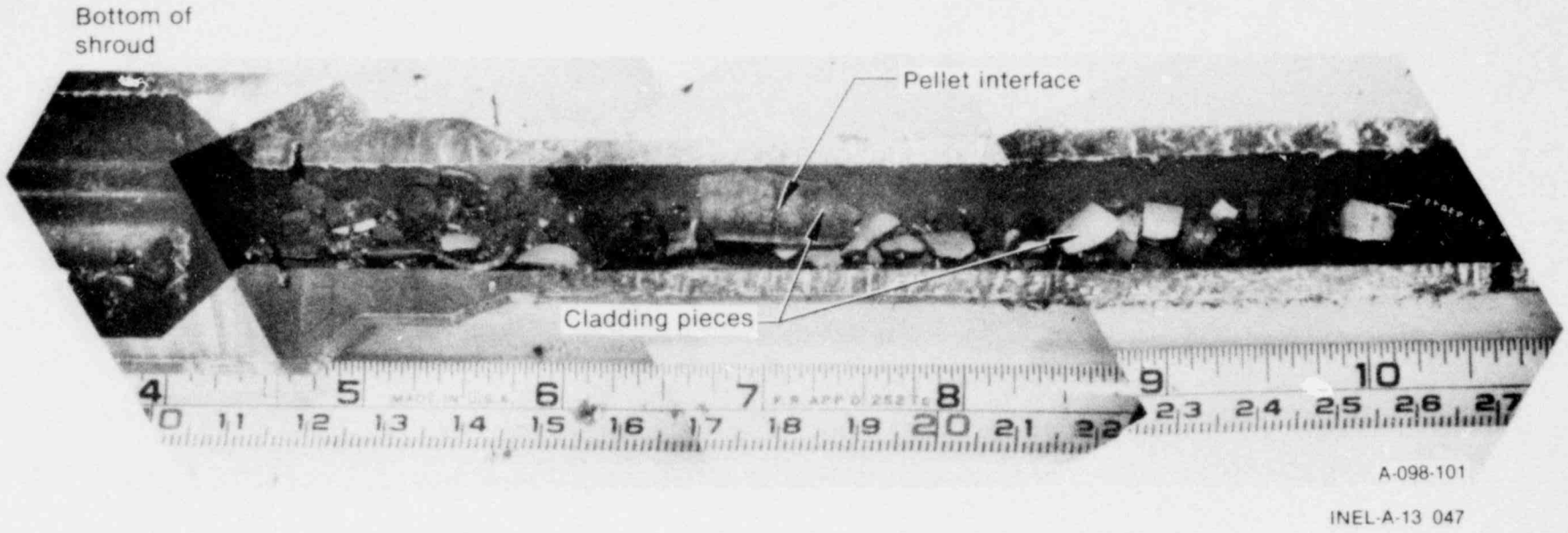


Fig. 16. Overall view of broken cladding pieces in the lower shroud (end cap) region.

Metallurgical estimates of cladding and fuel temperatures were obtained in order to help characterize the operating behavior of the fuel rod. The cladding temperatures at various axial and azimuthal positions were determined by either (a) correlation of cladding microstructures to specific phase-transformations in zircaloy or (b) calculation on the basis of the external $ZrO_2$ and the adjacent oxygen-stabilized alpha layer thickness. The fuel surface peak temperatures were calculated from the fuel melt radius and local power with a function of the form[19]

$$\frac{q}{4\pi} \propto \int k dT \qquad (1)$$

where

q = local heat flux
k = fuel thermal conductivity
T = temperature.

The fuel surface temperatures were used to estimate the cladding temperatures at the 0.30- and 0.67-m elevations. At the 0.30-m elevation, previously molten cladding was contained between layers of $ZrO_2$ on the inside and outside of the cladding. An estimate of the cladding temperature, using a constant thermal conductivity of $ZrO_2$ (2.4 W/m·K) and the pellet surface temperature, revealed that molten cladding would be expected. Apparently, steam ingress following failure caused an internal oxide layer to be formed, resulting in higher fuel and cladding temperatures at this elevation. Local cladding structural integrity was maintained by the shell of $ZrO_2$ around the molten zircaloy core. If the molten cladding had been formed prior to the rod failure (and buildup of an internal $ZrO_2$ layer), the rod section would probably not have remained intact. At the 0.67-m elevation, no molten cladding was observed. The cladding temperature estimate using the calculated pellet surface temperature agreed well with the 1580-K average obtained from the measured reaction layer thickness and oxide kinetics relationship. The cladding and fuel surface temperature estimates obtained metallurgically are shown graphically in Figure 17 for samples at known elevations.

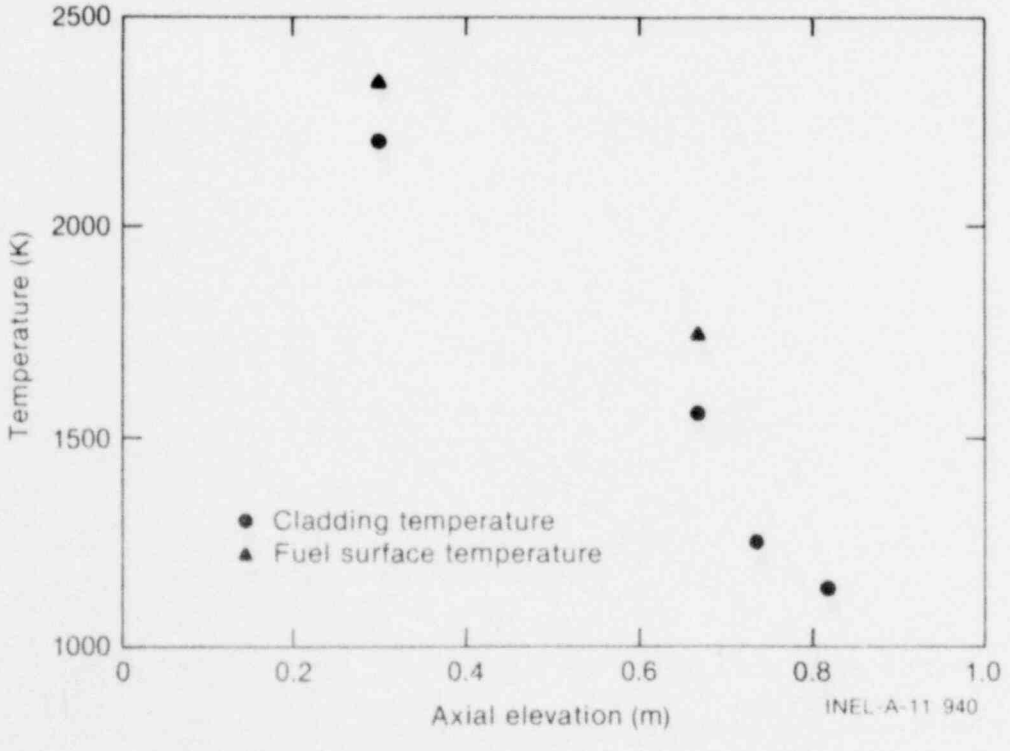


**Fig. 17. Posttest estimated cladding and fuel temperatures relative to the bottom of the fuel stack.**

A circumferential temperature gradient of approximately 200 K was observed in the cladding at two axial elevations (0.67 and 0.74 m above the bottom of the fuel stack). The common orientation of the gradient at both elevations suggests that the gradient was caused by postfailure asymmetry of the upper rod section within the shroud or by thermocouple leads attached to the rod. No circumferential variation in rod power, and subsequently in cladding temperatures, would be expected in the single-rod test configuration.

# IV. DISCUSSION OF EXPERIMENT RESULTS

Test PCM-1 was conducted to evaluate the film boiling behavior of a light-water-reactor-type fuel rod operated for a time beyond failure with large local regions of molten fuel, and to evaluate the consequences of the continued operation. Interpretation of the fuel rod behavior is qualitative in nature due to the severe operating conditions and the subsequent damage to the test rod. This section integrates the available instrumentation response and posttest examination information to provide an assessment of the fuel rod behavior during the Test PCM-1 DNB phase. New information obtained from the experiment is also discussed in this section.

## 1. SUMMARY OF FUEL ROD BEHAVIOR RESULTS

The response of the Test PCM-1 fuel rod prior to failure was similar to that observed during previous PCM experiments conducted at less severe conditions. The film boiling zone progressed from the upper rod portion (approximately 0.78 m above the bottom of the fuel stack) to lower elevations, stabilizing initially with approximately 0.4 m of the rod in film boiling. A cladding peak temperature of approximately 1750 K was calculated prior to the power adjustment at 283 s. During the power adjustment to 77.8 kW/m, the cladding temperatures and the extent of film boiling on the rod increased. A cladding peak temperature between 1850 and 1900 K was calculated for the remainder of the nuclear testing.

Fuel rod failure occurred 520 s after the start of the Test PCM-1 power ramp. The time to failure corresponds to a film boiling time at the peak temperature location of approximately 470 s. The mechanism of failure was probably cladding embrittlement due to the cladding-steam and cladding-fuel oxidation reactions. The equivalent cladding reacted was probably near 24% (100% of the wall thickness) at the failure time. Cladding failure due to molten fuel-cladding interaction is not probable. No energetic molten fuel-coolant interaction was observed, even though areas with 85% molten fuel were observed in the failed region. The lower fuel rod segment dropped down 2.7 mm in the shroud following failure. Breakup of highly embrittled cladding sections probably began shortly after the rod failure due to changes in the intrashroud geometry.

Additional breakup of the fuel rod and possible fragmentation of some of the exposed (to coolant) fuel pieces occurred following the rod failure. Cladding collapse onto the fuel stack restricted the internal coolant exposure to a local region near the fuel rod fracture surfaces. Internal cladding oxidation near fracture surfaces caused insulation of the rod, resulting in higher local fuel and cladding temperatures than those observed in the higher power regions where at-power cladding breakup occurred. Previously molten cladding between a shell of $ZrO_2$, and higher fuel temperatures in fuel pieces with cladding attached implies that higher fuel and cladding temperatures occurred following rod failure, since an internal $ZrO_2$ layer would not be expected from the fuel-cladding reaction. Circumferential cladding temperature gradients on the upper segment of the failed rod were probably caused by asymmetry after the initial failure. Breakup of the rod during nuclear operation did not inhibit the coolability of the single-rod assembly.

Rewet of the rod allowed gas communication between the intact rod sections and the fracture locations due to contraction of the fuel away from the cladding. Energetic reactions were not observed as a result of the fuel-coolant interaction. Additional rod breakup and relocation of fracture pieces resulted in an 80% shroud flow blockage following rewet. However, intact rod segments at the top and bottom of the rod with as much as 100% of the cladding reacted did not break up upon rewet. Fuel fragmentation resulted in 24% of the original fuel stack mass being transported from the shroud by the coolant flow. Fuel fragmentation and powdering[20] probably occurred due to thermal shock upon rewet.

## 2. NEW INFORMATION OBTAINED FROM TEST PCM-1

Test PCM-1 was the first experiment to be conducted under film boiling conditions for a significant time beyond fuel rod failure. The uniqueness of the experiment provided information in areas of fuel rod

behavior which previously had not been obtained in a nuclear environment. Observations obtained from Test PCM-1 which represent new information are:

(1) The at-power failure mechanism of the rod was most likely cladding embrittlement. The time in high temperature film boiling operation would result in nearly complete conversion of the cladding to either $ZrO_2$ or oxygen-stabilized alpha-zircaloy at the failure time. Molten fuel in the high power region (estimated to be about 50% of the fuel) either (a) did not contact the cladding, or (b) was extruded through fuel cracks and contacted the cladding but did not result in failure.

(2) The time to rod failure was 520 s after the start of the power ramp. The failure time corresponds to 496 s after the first indication of film boiling and to approximately 470 s of film boiling conditions at the peak power elevation.

(3) The fuel rod failure resulted in fracture of the rod and separation of the rod segments.

(4) Rod fracture and ensuing breakup did not significantly affect the coolability of the single-rod assembly during nuclear operation.

(5) Energetic molten fuel-coolant interaction was not indicated as a result of the failure and subsequent breakup of the rod.

(6) Cladding collapse onto the fuel stack isolated the fuel rod plenum from the failure location. Posttest evidence of steam ingress for a distance greater than the length of three fuel pellets in the intact cladding regions was not observed[4].

(7) Rewet of the failed rod caused additional rod breakup and gas (or water) communication between the failure location and fuel rod plenum to be established. Some intact cladding which had been completely oxidized to $ZrO_2$ survived the thermal shock of rewet.

The implications of the new information obtained from Test PCM-1 are summarized in the following section.

# V. CONCLUSIONS

The objective of Test PCM-1 was to operate a PWR-design fuel rod in film boiling for a time beyond failure with large local regions of molten fuel, and to evaluate the postfailure behavior. Specific areas of investigation were (a) the time of test rod failure, (b) the mechanism of failure, (c) the potential for energetic molten fuel-coolant interaction and molten fuel related rod failure, and (d) the consequences of operating a rod in film boiling for a significant time following failure. Specific conclusions and implications of the new information obtained from the experiment are as follows.

(1) The fuel rod failed due to cladding embrittlement after approximately 470 s of film boiling operation at the peak temperature elevation. The rod failure time corresponds to the time required to convert nearly all of the cladding wall to $ZrO_2$ and oxygen-stabilized alpha-zircaloy. Molten fuel contact with the cladding (if it occurred) did not result in early failure of the rod.

(2) Energetic molten fuel-coolant interactions (vapor explosions) did not occur as a result of rod failure or subsequent breakup.

(3) Rod failure and breakup did not significantly affect the coolability of the Test PCM-1 single-rod geometry during nuclear operation. Flow blockage in a bundle geometry (unirradiated rods) would not be expected during a PCM-1-type scenario until rewet of the highly embrittled rods occurred.

(4) Fuel shattering resulted in the washout of 24% of the fuel stack through the shroud screens (76-μm-mesh size), suggesting that thermal-shock-induced fuel powdering occurred rather than intimate molten fuel and coolant contact.

# VI. REFERENCES


1. United States Nuclear Regulatory Commission, Reactor Safety Research Program, *A Description of Current and Planned Reactor Safety Research Sponsored by the Nuclear Regulatory Commission's Division of Reactor Safety Research*, NUREG-75/058 (June 1975).

2. P. E. MacDonald et al, "Response of Unirradiated and Irradiated PWR Fuel Rods Tested Under Power-Cooling-Mismatch Conditions," *Nuclear Safety, 19(4)* (August 1978) pp 440-464.

3. D. E. Thornton and D. H. Schwieder, *Experiment Data Report For Test PCM-1 (Power-Cooling-Mismatch Test Series)*, NUREG/CR-0292, TREE-1233 (September 1978).

4. B. A. Cook, *Fuel Rod Material Behavior During Test PCM-1*, NUREG/CR-0757, TREE-1333 (June 1979).

5. R. N. Oehlberg, W. V. Johnston, J. A. Dearien, "FRAP Fuel Behavior Computer Codes," *Nuclear Safety, 19 (5)* (September-October 1978).

6. A. D. Appelhans, A. S. Mehner, W. J. Quapp, "Power Burst Facility Fission Product Detection System," *Transactions of the American Nuclear Society, 1978 Annual Meeting, Vol. 28* (1978).

7. R. B. Roemer, "The Effect of Power Transients on the Peak Heat Flux," *International Journal of Heat and Mass Transfer, 12* (1969) pp 953-964.

8. S. L. Seiffert, *Power-Cooling-Mismatch Test Series, Test PCM-2 Postirradiation Examination*, TREE-NUREG-1069 (March 1977).

9. S. L. Seiffert, *Power-Cooling-Mismatch Test Series, Test PCM-3 Postirradiation Examination*, TREE-NUREG-1187 (December 1977).

10. D. W. Croucher et al, *Irradiation Effects Test Series, Tests IE-5 Test Results Report*, TREE-NUREG-1130 (January 1978).

11. S. L. Seiffert and R. R. Hobbins, *Oxidation and Embrittlement of Zircaloy-4 Cladding from High Temperature Film Boiling Operation*, NUREG/CR-0517, TREE-1327 (April 1979).

12. R. E. Pawel, "Diffusion in a Finite System with a Moving Boundary," *Journal of Nuclear Materials, 49* (1973/74) pp 281-290.

13. R. E. Pawel, "Oxygen Diffusion in Beta Zircaloy During Steam Oxidation," *Journal of Nuclear Materials, 50* (1975) pp 147-258.

14. S. L. Seiffert and T. F. Cook, *Power-Cooling-Mismatch Test Series, Test PCM-4 Postirradiation Examination*, NUREG/CR-0138, TREE-1230 (July 1978).

15. J. V. Cathcart et al, *Zirconium Metal-Water Oxidation Kinetics IV. Reaction Rate Studies*, ORNL/NUREG-17 (August 1977).

16. P. Hofmann and C. Politis, "Chemical Interaction Between $UO_2$ and Zry-4 in the Temperature Range Between 900 and 1500°C," *4th International Conference on Zirconium in the Nuclear Industry, Stratford-upon-Avon, England, June 26-29, 1978.*

17. D. O. Hobson and P. L. Rittenhouse, *Embrittlement of Zircaloy-Clad Fuel Rods by Steam During LOCA Transients*, ORNL-4758 (January 1972).

18. C. J. Scatena, *Fuel-Cladding Embrittlement During A Loss-of-Coolant Accident*, NEDO-10674 (October 1972).

19. M. S. El-Genk, *An Assessment of Fuel Melting, Radial Extrusion, and Cladding Thermal Failure During a Power-Cooling-Mismatch Event in Light Water Reactors*, NUREG/CR-0500, TREE-1270 (May 1979).

20. A. W. Cronenberg and T. R. Yackle, *An Assessment of Intergranular Fracture within Unrestructured $UO_2$ Fuel Due to Film Boiling Operation*, NUREG/CR-0595, TREE-1330 (March 1979).

DISTRIBUTION RECORD FOR NUREG/CR-0907

(TREE-1374)

Internal Distribution

1 - R. J. Beers, ID

2 - P. E. Litteneker, ID

3-5 - LNEL Technical Library

6-10 - Author

11-50 - Special Internal

External Distribution

51-52 - S. Levine, Director
Office of Nuclear Regulatory Research, NRC
Washington, D.C. 20555

53-59 - Special External

60-399 - Distribution under R3, Water Reactor Safety Research - Fuel Behavior

# DOCUMENT/ PAGE PULLED

# ANO. 7910020650

NO. OF PAGES 1
MICROFICHE

REASON:

☐ PAGE ILLEGIBLE:

☐ HARD COPY FILED AT: PDR CF
OTHER _____

☐ BETTER COPY REQUESTED ON ____/____/____

☐ PAGE TOO LARGE TO FILM:

☐ HARD COPY FILED AT: PDR CF
OTHER _____

☐ FILMED ON APERTURE CARD NO. _____

1070 190